Chu, D., Tong, J., Bottjer, D. J., Song, H., Song, H., Benton, M. J., Tian, L., & Guo, W. (2017). Microbial mats in the terrestrial Lower Triassic of North China and implications for the Permian-Triassic mass extinction. *Palaeogeography, Palaeoclimatology, Palaeoecology*, *474*, 214–231. https://doi.org/10.1016/j.palaeo.2016.06.013

Microbial mats in the terrestrial Lower Triassic of North China and implications for the Permian-Triassic mass extinction

Daoliang Chu[1], Jinnan Tong[1*], David J. Bottjer[2], Haijun Song[1], Huyue Song[1], Michael J. Benton[3], Li Tian[1], Wenwei Guo[1]

[1]State Key Laboratory of Biogeology and Environmental Geology, School of Earth Sciences, China University of Geosciences, Wuhan 430074, China

[2]Department of Earth Sciences, University of Southern California, Los Angeles, CA 90089, USA

[3]School of Earth Sciences, University of Bristol, Bristol, BS8 1RJ, UK

*Corresponding author: jntong@cug.edu.cn (J.N.Tong).

Abstract

Microbial mats have been reported repeatedly in marine Lower Triassic rocks, but scarcely mentioned in post-mass extinction terrestrial facies. Here, we report from the terrestrial Lower Triassic Liujiagou Formation in North China the presence of five kinds of microbially induced sedimentary structures (MISS) or sedimentary surface textures, including "old elephant skin" textures, wrinkle structures, palimpsest ripples, "*Manchuriophycus*" structures and sand cracks. These terrestrial microbial communities adapted not only to periodically desiccated conditions, but also to the storm-dominated palaeoenvironments in the Liujiagou Formation. The Permian-Triassic mass extinction (PTME) in North China is marked by the die-off of plants, disappearance of coal beds, extinction of pareiasaurs among tetrapods, decreased bioturbation levels and a dramatic change of sedimentary systems through the Sunjiagou Formation. The Sunjiagou Formation recorded the turnover from an ever-wet to a progressively drier and hotter climate and it spans the PTME in North China. Following this mass extinction, MISS became much more common and widespread,

suggesting that the mass extinction provided favourable biological and environmental conditions for the development of the MISS in terrestrial ecosystems, especially the decreased bioturbation intensity and grazing pressure associated with increased temperature and climatic drying. In the upper part of the Liujiagou Formation and overlying Heshanggou Formation, the disappearance of MISS coupled with increased bioturbation might indicate an improvement of terrestrial ecosystems and the beginning of the Triassic biotic recovery. However, as the investigation of MISS in space and time through the geological record is in its early stages, further geobiologic and geochemical studies, as well as high-precision isotopic dating from Permian-Triassic terrestrial successions, are needed to fully reveal the timing and pattern of the Early Triassic terrestrial ecosystem reconstruction.

Keywords: Microbial mat; Microbially induced sedimentary structures (MISS); Early Triassic; Terrestrial ecosystem; Permian-Triassic mass extinction (PTME); North China

1. Introduction

Microbially induced sedimentary structures (MISS) were produced by the interaction between microbial activities and physical sedimentary processes in ancient siliciclastic and carbonate depositional systems (Hagadorn and Bottjer, 1997; Noffke et al, 2001; Noffke, 2009, 2010). These structures are always preserved on the upper surfaces of the substrate, which now form rock bedding planes, but it is hard to observe the original microbial mats because of destruction during diagenetic processes that followed MISS formation. Analysis of the formation mode and internal textures of these sedimentary structures, as well as comparison with modern microbial mat structures suggest that the formation and preservation of these structures have a direct relationship with the presence of microbial mats (Hagadorn and Bottjer, 1997). Furthermore, MISS are common sedimentary features in

Proterozoic-Cambrian strata extending back to the Early Archean (e.g. Hagadorn and Bottjer, 1997, 1999; Gehling, 1999; Noffke et al., 2002, 2003, 2006; Schieber et al., 2007; Meyer et al., 2014), most probably due to the lack of bioturbation that inhibits the formation and preservation of biomats and associated structures. In addition, the occurrence of MISS provides valuable evidence for the detection of early life and reconstruction of environments in the Precambrian (Noffke et al., 2003). So far, several authors have studied Precambrian MISS in continental facies (Prave, 2002; Collow et al., 2011; Simpson et al., 2013; Wilmeth et al., 2014; Strother and Wellman, 2015), and they have argued that microbial communities were flourishing and inhabited continental settings at that time.

In the Phanerozoic, most studies have suggested that sedimentary structures related to microbial communities became more common as a response to periods of lower benthic biodiversity and reduced bioturbation, including a variety of unusual sedimentary structures (Sepkoski et al., 1991; Schubert and Bottjer, 1992; Grotzinger and Knoll, 1995; Wignall and Twitchett, 1999; Whalen et al., 2002; Sheehan and Harris, 2004; Calner, 2005; Pruss et al., 2006; Mata and Bottjer, 2009; Buatois et al., 2013; Chu et al., 2015; Ibarra et al., 2016; Peterffy et al., 2016; Rakociński and Racki, 2016). However, Davies et al. (2016) recently demonstrated that MISS have been reported more from Phanerozoic than Precambrian strata, and exhibit a pan-environmental and almost continuous record since the Archean, while the perception that MISS are restricted to exceptional intervals of Earth history could arise from a sampling and publication bias. In addition, abiotic and physicochemical sedimentary processes may also create morphologically similar features to MISS, hindering their accurate identification (e.g. Mcloughlin et al., 2008; Davies et al., 2016). Therefore, more original observations of MISS from multiple depositional systems should be collected to re-evaluate the relationship between biotic crises and the flourishing of MISS after these events.

As the greatest crisis of the Phanerozoic, the Permian-Triassic mass extinction (PTME) is

of particular interesting to geologists. This event wiped out over 90% of marine species, and most terrestrial vertebrate and plant species, and brought about a whole-scale restructuring of ecosystems (Erwin, 1993; Retallack, 1995; Looy et al., 1999, 2001; Song et al., 2013; Benton and Newell, 2014; Benton, 2015). The diversity of marine invertebrates declined dramatically (Alroy et al, 2008), and bioturbation returned to Precambrian levels (Knaust, 2010). The terrestrial PTME is confirmed by the significant turnover and loss of life on land from global-scale data, such as tetrapods, insects and plants (Retallack et al., 1996; Grauvogel-Stamm and Ash, 2005; Hermann et al., 2011; Benton and Newell, 2014; Cascales-Miñana and Cleal, 2014; Cascales-Miñana et al., 2015; Yu et al., 2015), though the position of the terrestrial Permian-Triassic boundary is disputed in different regional basins (e.g. Botha and Smith, 2006; Taylor et al., 2009; Gastaldo et al., 2015). Plant diversity had declined substantially through the PTME followed by the Early Triassic "coal gap" (Veevers et al., 1994; Retallack et al., 1996, 2011; Looy et al., 1999, 2001; Rees, 2002; Retallack, 2013). Furthermore, the significant turnover of the terrestrial sedimentary system and the dramatic collapse of soil systems associated with persistent warming, arid climate and enhanced terrestrial weathering have been documented globally during the PTME (Newell et al., 1999; Ward et al., 2000, 2005; Michaelsen, 2002; Miall and Jones, 2003; Arche and LopezGomez, 2005; Retallack, 2005; Algeo and Twitchett, 2010; Algeo et al., 2011; Smith and Botha-Brink, 2014; Metcalfe et al., 2015; Schneebeli-Hermann et al., 2015; Song et al., 2015). Most studies suggest that the destruction of terrestrial ecosystems happened simultaneously with the decline in marine diversity during the Permian-Triassic transition (Twitchett et al., 2001; Shen et al., 2011; Metcalfe et al., 2015; Zhang et al., 2015; Chu et al., in review). Deposits of this unusual period are characterized by the presence of flat-pebble conglomerates (Wignall and Twitchett, 1999), thin-bedded limestones (Pruss et al., 2005), carbonate seafloor fans (Woods, 1999), and siliciclastic microbial-mat related wrinkle

structures (Pruss et al., 2004; Chu et al., 2015). Microbial buildups and mats dominated the seabed after the Permian-Triassic crisis, and these microbe-dominated marine ecosystems lasted for about 5–6 Myr in the Early Triassic, linked to the depression of bioturbation and/or to long-term unusual environmental conditions (Chen and Benton, 2012). Most studies that mentioned these unusual sedimentary structures from the Lower Triassic were restricted to marine carbonate and siliciclastic rocks (e.g. Schubert and Bottjer, 1992; Lehrmann, 1999; Wignall and Twitchett, 1999; Woods, 1999; Pruss et al., 2004, 2005, 2006; Pruss and Bottjer, 2004; Abdolmaleki and Tavakoli, 2016). However, less is known about specific changes in terrestrial microbial ecosystems during the PTME and its aftermath, though specific MISS have been reported in terrestrial Lower Triassic rocks (Wehrmann and Gerdes, 2012; Chu et al., 2015; Tu et al., 2016).

Terrestrial Permian-Triassic successions are well exposed and widely distributed in the Shanganning Basin and its surrounding area, such as Shanxi, Shaanxi, Henan, and Ningxia Provinces in North China, characterized by inland fluvial and lacustrine siliciclastic redbeds. Complete terrestrial Permian-Triassic sections in North China have been little studied, and yet these sections contain important clues for a better understanding of terrestrial ecosystems. Following our report of microbial-related wrinkle structures from the Lower Triassic of the Dayulin section, Henan Province, North China (Chu et al., 2015), Tu et al. (2016) described some kinds of MISS from the same section and suggested that microbes also proliferated in terrestrial ecosystems in the aftermath of the PTME. The MISS in terrestrial siliclastic facies seem to coincide with the "unusual sedimentary record" in marine settings, which were associated with the end-Permian mass extinction events (Pruss et al., 2004, 2005, 2006; Baud et al., 2007; Chen et al., 2014). Consequently, MISS would be expected to be observed in more terrestrial facies and might be taken as an indicator of the Permian-Triassic boundary in terrestrial stratigraphical sequences. Here we present some more evidence for

126 microbial-mat-related sedimentary structures from the Lower Triassic shallow-shore
127 lacustrine siliciclastic deposits in North China. In addition, this study presents a more detailed
128 analysis of terrestrial extinction on the basis of previous and new biostratigraphic,
129 sedimentological, and lithological data from the studied area to reveal the timing and pattern
130 of the PTME in North China. Furthermore, we discuss the relationship between the PTME
131 and the Early Triassic flourishing of MISS.
132
133 **2. General lithostratigraphy and study sections**
134 The Upper Permian to Lower Triassic sedimentary sequence in North China is
135 represented by the Shiqianfeng Group, which consists of the Sunjiagou, Liujiagou and
136 Heshanggou formations, in ascending order (Fig. 1). The Sunjiagou Formation consists of
137 fine-grained sandstones and thinly interbedded siltstones in the lower part and reddish
138 siltstone beds, mudstone laminae and interbedded sandstone and marlstone beds in the upper
139 part (Fig. 2A, B). Intensive bioturbation and the *Ullmannia bronnii-Yuania magnifolia* plant
140 fossil assemblage, which is known as the youngest Palaeozoic flora in North China (Wang
141 and Wang, 1986; Chu et al., 2015), occur in the lower part of the formation. In previous
142 stratigraphic studies, the base of the Sunjiagou Formation was dated variously from middle
143 Wuchiapingian to basal Changhsingian, and the Sunjiagou Formation was considered to cover
144 the entirety of the Changhsingian stage from the evidence of lithostratigraphy, palaeobotany
145 and palynology (Wang and Wang, 1986; Stevens et al., 2011; Zhang et al., 2012; Liu et al.,
146 2015), though no reliable age-diagnostic fossils are found in the upper part of the formation.
147 The overlying Liujiagou Formation comprises reddish and brown-reddish, fine-grained
148 sandstones with siltstones and fine-grained conglomerates, bearing abundant ripple marks and
149 cross bedding (Fig. 2C–F), and characterized by lacustrine wrinkle structures but an absence
150 of bioturbation, and deposited in a lake shore or fluvial environment (Chu et al., 2015; Tu et

al., 2016). The typical Early Triassic plant fossil *Pleuromeia* occurs in the upper part of the Liujiagou Formation, and these are more widely distributed in the Lower Triassic strata (Wang and Wang, 1982; Wang, 1996; Retallack, 1997; Grauvogel-Stamm and Ash, 2005). The Heshanggou Formation consists of brown-reddish and purple mudstone laminae and siltstone beds with interbedded sandstone beds with diverse ichnofossils, such as *Planolites*, *Psilonichnus*, *Scoyenia*, *Skolithos*, and *Taenidium*, deposited in a shallow-shore lake palaeoenvironment.

The samples of MISS and other sedimentary surface textures were collected from the Liujiagou Formation of the Dayulin and Liulin sections, which are well exposed in Henan and Shanxi provinces, North China (Fig. 1). The Dayulin section is situated near Yiyang County, Luoyang City, Henan Province (Fig. 1B). It includes successive Late Permian to Early Triassic terrestrial siliciclastic deposits from the Sunjiagou, Liujiagou and Heshanggou formations (Fig. 1C). We collected abundant plant fossils and ichnofossils from the lower part of the Sunjiagou Formation. Diverse MISS are mainly preserved on sandstone bed tops of the lower to middle part of the Liujiagou Formation, associated with abundant ripple marks and cross bedding, including hummocky cross-stratification and, in some cases, infrequent ichnofossils such as *Planolites*. In contrast, the overlying Heshanggou Formation is characterized by diverse ichnofossils, but the absence of MISS in the massive siltstones and mudstones. The Liulin section outcrops along the highways on both sides of the Yellow River, extending from Wubu County of Shaanxi Province to Liulin County of Shanxi Province (Fig. 1B). It exposes continuous outcrop of the Sunjiagou, Liujiagou, and Heshanggou formations, and the overlying Middle–Upper Triassic strata are exposed on both sides of the Yellow River (Fig. 2C). The Sunjiagou Formation consists of interbedded sandstones and mudstones or siltstones, with the last appearance of coal beds occurring in the lower part associated with plant fossil fragments (Fig. 1C). MISS were observed and collected

on sandstone bedding surfaces from the middle part of the Liujiagou Formation in the Liulin section. Similarly, the overlying Heshanggou Formation is composed of siltstone beds and mudstone laminae with interbedded sandstone beds, and characterized by diverse ichnofossils, but devoid of MISS.

3. Methods

We measured stratigraphic sections and collected plant fossils in the field. In addition, trace fossils were investigated bed-by-bed and the bedding plane bioturbation index (BPBI) was measured following the method of Miller and Smail (1997). Bedding planes containing MISS were described in detail and samples were collected at each locality. Two detailed lithological logs are provided to mark the positions of the fossils and MISS samples recovered. All the features were photographed with a Canon EOS 7D digital camera. Four samples were slabbed with a cut perpendicular to the bedding surface to study changes in grain size. A total of 29 thin sections were produced for petrological analysis using standard techniques. These were then examined and photographed using a Leica DM-750P microscope equipped with an automatic camera stack-image system. Four slabs and three thin sections were employed for ultramicroscopic studies under a Hitachi SU8010 scanning electron microscope (SEM) with iXRF EDS. All samples in this study are stored in the palaeontological collection of the State Key Laboratory of Biogeology and Environmental Geology, China University of Geosciences, Wuhan (BGEG).

4. Major types of MISS and interpretation

Diverse MISS were observed and collected from the Liujiagou Formation in the two sections. Here we document all the types of MISS we observed at the studied sections following the classification scheme of Schieber et al. (2007), including “old elephant skin”

textures, wrinkle structures, palimpsest ripples, "*Manchuriophycus*" structures and sand cracks. In addition, we employ the classification scheme proposed by Davies et al. (2016) for distinguishing abiogenic and biogenic sedimentary surface textures in the field, Category A are demonstrably not microbially induced in origin, Category B are demonstrably microbially induced, and Category ab represents structures for which there is no clear evidence to support either origin.

4.1. "Old elephant skin" textures

4.1.1. Description

"Old elephant skin" (OES) textures were observed on fine sandstone bedding surfaces in the middle part of the Liujiagou Formation at Liulin (Fig. 3, Category B). They are preserved as convex epireliefs with polygonal texture and projecting 2–5 mm from the bedding surface (Fig. 3D). Dark clay laminae overlying the surface have been observed by microscopic study of thin sections (Fig. 4). In addition, SEM images show that the superposed clay laminae wrapped around the quartz grains.

4.1.2. Interpretation

The OES structure was described as "a surface corrugation of a sandstone bed which provides a quasi-polygonal texture in the rock record" (Bottjer and Hagadorn, 2007), and it was considered as a kind of specific wrinkle structure. Bottjer and Hagadorn (2007) suggested that this type of structure might form when mats provided a veneer between the lithologically identical overlying and underlying beds. The OES therefore should represent microbial mat surface features that have been induced by the microbial mat itself (Hagadorn and Bottjer, 1997, 1999; Gehling, 1999; Gerdes et al., 2000). In this study, the OES preserved as positive epireliefs on sandstone bed tops associated with ripple marks (Fig .3), and forming in both the

ripple crests and troughs, might suggest that a microbial mat protected the areas where the original ripple set is preserved.

4.2. Wrinkle structures

4.2.1. Description

A total of three wrinkle structure types were recognized through studies of morphology and microscopic characteristics, including cross-cutting wrinkle structures, parallel wavy wrinkle structures and bulge-like wrinkle structures (e.g. Chu et al., 2015). Cross cutting wrinkle structures (Banerjee and Jeevankumar, 2005) are preserved as bifurcating and frequently interconnected crests on bed tops of fine sandstones, while one set of wrinkles cuts across another set at a low angle (Fig. 5A–C). The crests are 2–5 mm in height, and 2–6 mm in width. Opaque laminar clays were observed on the surfaces of the wrinkles in Figure 5A from thin section microscopic features (Fig. 6C). Fine-grained quartz grains are abundant in the surface laminae as floating grains, and these differ in size from normal grains in the thin sections and slabs (Fig. 6B, C). SEM investigations show that the floating grains are enclosed by curved, continuous and thin laminar clays, while Energy-dispersive X-ray spectroscopy (EDS) shows that these submicroscopic features are highly enriched in silica and aluminium.

Parallel wavy wrinkle structures are preserved as sinuously curved continuous crests, separated by parallel narrow troughs, on the upper surfaces of fine sandstone beds (Fig. 5D–F). The height of individual crests usually ranges from 1–4 mm, and their spacing from 10–15 mm. Microscopic thin sections perpendicular to the structural trend show that the clay laminae are completely encased in sediment above and below, representing the complete structure of the wrinkles (Fig. 6D, E). Bulge-like wrinkle structures are preserved as elongated to subrounded bulges, characterized by patches of convex epireliefs, 2–6 mm in width and irregularly distributed, and separated from each other by narrow grooves, on the

upper surfaces of fine sandstone beds (Fig. 6F, 7A). Opaque laminar clays are observed on the surfaces of the wrinkles in thin section (Fig. 6G–I). In addition, bulges with similar geometry and orientation are distributed along the extension directions of ripple crests (Fig. 7B), suggesting successful protection by the overlying microbial mats against hydrodynamic damage.

4.2.2. Interpretation

Wrinkle structures have been reported repeatedly from shallow marine settings in the Precambrian and the aftermaths of Phanerozoic extinction events (e.g. Hagadorn and Bottjer, 1997; Pruss et al., 2004, 2006; Banerjee and Jeevankumar, 2005; Mata and Bottjer, 2009; Banerjee et al., 2010; Lan et al., 2013), but rarely mentioned in rocks recording terrestrial settings (but see Chu et al., 2015; Tu et al., 2016). In this study, wrinkle structures are one of the most common MISS types in the studied localities. We have found various forms of wrinkle structures in the lower to middle part of the Liujiagou Formation at Dayulin, and in the middle part of the Liujiagou Formation at Liulin. Thin sections show the preservation of a clay veneer and floating quartz grains, which suggest possible grain-trapping and binding from the surrounding environment (Hagadorn and Bottjer, 1997; Banerjee and Jeevankumar, 2005). The preservation of bulge-like wrinkles and their particular peripheries reflect subsurface morphological features developed beneath a microbial mat (Porada and Bouougri, 2007). Recently, Mariotti et al. (2014) described one of the best experimentally constrained mechanisms for the formation of wrinkle structures and similar structures, that “pits form when porous mat aggregates anchor to the bed, oscillate and scour the sand, and ridges form when the oscillatory rolling, dragging and hopping of rounded mat fragments transport sand grains from depressions to bumps”. In addition, observation of the formation of modern ridge- and pit-shaped wrinkle structures indicates that waves with a small orbital amplitude at the

bed surface move the microbial fragments and thereby produce linear sand ridges and rounded scour pits at wavelengths within hours, but not move sand grains directly.

4.3. Palimpsest ripples structures

4.3.1. Description

Palimpsest ripple structures are preserved as two successive sets of ripples that crossed at a specific angle on the bed tops, and the crests of each set are spaced 20–30 mm apart (Fig. 7C). In these cases, the overlapping of secondary ripples onto primary ripples formed diamond-shaped structures, with isolated patches in which there is no overlap (Fig. 7C, D). The crests of the two sets of ripples are generally flat or subrounded, and coalesced bulges or quasi-polygonal textures resemble bulge-like wrinkle structures or OES in appearance (Fig. 7D). Dark clay laminae overlying the surface are observed in microscopic thin sections, and microbial mats are inferred to have covered these sandy rippled surfaces in the aftermath of the formation of the palimpsest ripple structures, and so protected the lower layers.

4.3.2. Interpretation

The two separate sets of ripples were likely formed by storms or wind-reinforced tides in two depositional events, and a microbial mat must have developed between the two sandy beds with ripples, protecting the earlier ripples from being destroyed by later reworking. This biostabilization or mat binding effect allows two or more sets of ripples to be preserved on the same bedding plane (Pflüger, 1999; Noffke et al., 2001; Bottjer and Hagadorn, 2007; Lan and Chen, 2013). However, multi-directional ripples also can form in modern tidally influenced environments without any microbial mats, generated by different oscillation directions in shallow water (Davies et al., 2016).

301 **4.4. "*Manchuriophycus*" structures**

302 **4.4.1. Description**

303 "*Manchuriophycus*" structures represent a special type of microbial shrinkage crack,
304 consisting of sinuous, circular, spiral or even figure-of-eight-shaped cracks with curving
305 positive patterns, which are usually confined to troughs between ripples on the rippled
306 surfaces of sandstone beds (Fig. 8). They were observed and collected in the lower part of the
307 Liujiagou Formation at Dayulin and in the middle part of the Liujiagou Formation at Liulin.
308 Individual crack fills with tapering ends vary from 2–4 mm in width and project 1–3 mm
309 from the bed surface.

310

311 **4.4.2. Interpretation**

312 Initially, "*Manchuriophycus*" was named as a Precambrian macrofossil (Endo, 1933;
313 Hofmann, 1967), but then it was reinterpreted as a physical sedimentary structure formed by
314 synaeresis shrinkage of clay veneers or by compaction and sediment foundering beneath
315 overlying sediments (Plummer and Gostin, 1981). A related explanation was that they formed
316 by shrinkage of strong and elastic microbial mats, but not the clay veneers (Gehling, 1999,
317 2000; Koehn et al., 2014). Considering that they are preferentially developed in the troughs of
318 flat-topped ripples, "*Manchuriophycus*" structures may form if microbial mats selectively
319 grew, or attained a greater thickness, in ripple troughs than on the crests (Schieber, 2007;
320 Eriksson et al., 2007; Lan and Chen, 2012; Buatois et al., 2013). In summary, the formation of
321 this structure is thought to relate to the selective growth of the microbial mat and its thickness
322 (Parizot et al., 2005).

323

324 **4.5. Sand cracks**

325 **4.5.1. Description**

Sand crack-fills were the most common microbial-induced features in the intertidal-supratidal zones of shallow marine and lacustrine environments in the Precambrian (Schieber, 2007; Eriksson et al., 2007; Callow et al., 2011; Lan and Chen, 2012, 2013; Simpson et al., 2013; Lan et al., 2015 and references therein), but have been less reported in the Phanerozoic. In this study, sand cracks with these peculiar morphological characteristics have been found in the lower and middle parts of the Liujiagou Formation in the two studied sections, and they exhibit a variety of geometries, such as pedate, mesh-like, spindle-shaped and rectangular to polygonal patterns (Fig. 9). Individual pedate crack fills vary from 20–40 mm wide and project 10–20 mm above the bed surface (Fig. 9A). Multiple small, mesh-like cracks are preserved as positive quasi-polygonal features that were formed by the mutual connection among crack-fills on sandstone bed tops. In some cases, multiple sets of crack-fills with specific widths and tapering ends indicate that several generations of shrinkage cracks developed as they formed (Fig. 9B). Spindle-shaped sand cracks are preserved as positive epireliefs within troughs and crests on the upper rippled surfaces of sandstones (Fig. 9C, D, category B). Sometimes, the spindle-shaped crack-fills are slightly deformed with curved patterns. Rectangular to polygonal synaeresis cracks are preserved on sandstone bed surfaces associated with the ripples, and these form "triple junction" incipient cracks without any cross-cut structure.

4.5.2. Interpretation

Microbial shrinkage sand cracks are easily confused with ichnofossils or purely physical desiccation cracks, unless they present specific morphological characteristics or indirect evidence for the former existence of cohesive biofilms or microbial mats in sandy deposits (Lan et al., 2015). In our study, no dark clay laminae or changes in grain size are observed in thin sections, which would be indirect evidence for the former existence of microbial mats.

However, considering their peculiar morphological characteristics, such as sinuous, doubly tapering, and sand-filled forms, these sand cracks may have been induced by microbial mat shrinkage, as they are significantly different from purely physical desiccation cracks. Furthermore, spindle-shaped sand cracks developed on wrinkle surfaces of sandstones (Fig. 9C, D), and opaque laminar clays are observed on the surfaces of the wrinkles (Fig. 9E), suggesting that the bedding surface was covered by a microbial mat during formation of the crack fills.

5. The Permian-Triassic terrestrial extinction in North China

We collected some typical Late Permian plant fossils, such as *Taeniopteris*, *Majonica*, *Ullmannia* and *Lobatannularia* (Fig. 10A–D), from the lower part of the Sunjiagou Formation, but no plant fossils were recorded in the overlying red sedimentary units at Dayulin. In addition, plant fossils, assigned to the genus *Ullmannia*, were found by Wang and Wang (1986) in the mid-upper part of the Sunjiagou Formation in the Liulin area, and these represented the last appearance of this typical Late Permian plant genus. Combining a survey of literature with original collections of Permian plant fossils in North China, a total of 19 genera and 32 species of Late Permian plants from the Sunjiagou Formation became extinct (Supplementary of Chu et al. 2015), corresponding closely to the PTME of plants. Furthermore, coal seams observed in the lower part of the Sunjiagou Formation at Liulin represent the last occurrence of coal in the Permian of North China (Fig. 10E). This has been attributed to the extinction of peat-forming plants associated with the arid climate and increasing temperature (Retallack et al., 1996). Among Late Permian tetrapods, six different pareiasaurs have been reported from the Shihezi and Sunjiagou formations in North China (Young and Yeh, 1963; Gao, 1983, 1989; Li and Liu, 2013; Xu et al., 2015), but re-analysis of all the original specimens shows that only three of these are valid, *Honania* in the Shihezi

Formation, and *Sanchuansaurus* and *Shihtienfenia* in the Sunjiagou Formation (Benton, 2016). In fact, pareiasaurs flourished from the Wordian to Changhsingian, but died out during the PTME (Benton, 2016). The level at which pareiasaurs disappear from the Sunjiagou Formation indicates the tetrapod extinction during the PTME. Meanwhile, the absence of metazoans and decreased bioturbation intensity in the upper part of the Sunjiagou Formation and Liujiagou Formation in North China correspond with each other, based on investigation of the fossils collected, literature surveyed and bioturbation index measured (this study; Chu et al., 2015; Tu et al., 2016; Fig. 11).

A distinct shift of lithology of the sedimentary facies can be observed. In the Sunjiagou Formation, the greyish-green, grey and dark grey alternating mudstones, siltstones and fine-grained sandstones in the lower part contrast markedly with the red, brown and purple mudstones, siltstones and fine-grained sandstones in the upper part. These then contrast with the red, brown and purple siltstone, sandstone and conglomerate beds of the overlying Liujiagou Formation. The lower part of the Sunjiagou Formation is characterized by vertical burrows, small-scale ripple cross bedding, plant fossils and infrequent coal seams (Fig. 10A–F), which indicate deposition in a swampy/lacustrine or river flat environment. The overlying Liujiagou Formation comprises red, brown and purple siltstones, sandstones and conglomerates frequently with large-scale cross-bedding, patches of minor angular poorly sorted green to maroon or red mud rock clasts and desiccation cracks (Fig. 10G, H), which contain a higher proportion of sandstone to shale than in the underlying Sunjiagou Formation. We interpret these massive sandstone units as having formed in a very shallow lake to a river flat environment, although the lower part suggests a storm-dominated shallow lake setting (Chu et al., 2015; Tu et al., 2016). The sedimentary record from the Sunjiagou Formation to the overlying Liujiagou Formation indicates a dramatic change of sedimentary system and a collapse of the terrestrial soil system. As mentioned above, the most probable causes of this

sedimentary system turnover, associated with enhanced soil erosion and terrestrial weathering, are the widespread die-off of plants and the decrease of vegetation coverage which is attributed to rapid global warming and persistent arid climate (e.g. Retallack et al, 1996, 2005; Looy et al., 1999, 2001; Ward et al., 2000; Newell et al., 2009; Benton and Newell, 2014; Benton, 2015).

In summary, the end-Permian biotic crisis was represented by the die-off of plant fossils, the disappearance of coal beds, the extinction of tetrapods including pareiasaurs, decreased bioturbation levels and a dramatic change of the sedimentary system coupled with the collapse of the terrestrial soil system in the Sunjiagou Formation, which corresponds to the first lithological unit of the Permian-Triassic red beds in North China (Fig. 11). The Sunjiagou Formation records the turnover from an ever-wet to a progressively drier and hotter climate, indicative of the terrestrial PTME in North China.

6. Discussion

6.1. How did the mass extinction affect the flourishing MISS: favourable conditions or essential conditions?

Following metazoan diversification and increased benthic bioturbation in the post-Cambrian, microbial sedimentary structures are commonly considered to be mainly restricted to exceptional intervals and anomalous environments associated with low levels of bioturbation and grazing (e.g. Calner, 2005; Pruss et al., 2006; Mata and Bottjer, 2009), but some studies suggest that in fact MISS existed in the depositional records of various environments throughout the Phanerozoic (e.g. Noffke and Chafetz, 2012; Carmona et al., 2012; Dai et al., 2015; Xing et al., 2016). However, the flourishing of MISS have been commonly and globally described from post-extinction intervals, suggesting that these occurrences are not coincidental, but do indicate a causal connection.

In most cases, a low level of bioturbation or grazing pressure is one of the most important determining factors in the original formation of MISS, and their later preservation, especially for surface features, due to the absence of destruction from biological interactions. However, considering the repeated and widespread presence of local environments with low levels of bioturbation and grazing throughout Earth history, it cannot be said that MISS only appear in the aftermath of biotic mass extinctions. In fact, changes in local sedimentary systems and depositional environments also provide favourable biological and environmental conditions for the formation and preservation of MISS. So, it should be said that a mass extinction, particularly where bioturbation has been reduced, can provide favourable conditions for thriving microbial communities and development of MISS, but not always. The essential factor for the presence of MISS is the amount of bioturbation. That is why MISS are found in brackish, marginal marine, intertidal, supratidal and lacustrine environments in the Precambrian as well as in the Phanerozoic, where metazoan bioturbation is commonly limited by stressful conditions (Hagadorn and Bottjer, 1997; Pruss et al., 2004, 2006; Schieber et al., 2007; Mata and Bottjer, 2009). However, normal marine subtidal environments in the Phanerozoic commonly have substantial bioturbation, and MISS are less common in those conditions. But, when bioturbation is reduced in subtidal environments for some reason, MISS may develop there, such as after a mass extinction, until bioturbation increases again to levels that preclude MISS. Thus, the essential factor is not mass extinctions but the presence and amount of bioturbation, which can be reduced for a variety of reasons, including mass extinctions.

For this study, the Sunjiagou Formation records the PTME and turnover of the sedimentary system, as well as significant climate change. Bioturbation was much reduced after this mass extinction, as indicated by our measurements of the bioturbation index from the Dayulin section (Fig. 11; Chu et al., 2015; Tu et al., 2016). MISS are widely distributed in

451 the post-crisis lower-middle part of the Liujiagou Formation, but absent in the underlying
452 richly bioturbated Sunjiagou Formation in North China. Therefore, decreased grazing
453 pressure, coupled with low-level bioturbation following the PTME, promoted the formation
454 and preservation of MISS.
455
456 **6.2. Distribution and depositional conditions of MISS at the studied area**
457 In this study, MISS were confined to the lower-middle part of the Liujiagou Formation in
458 the studied sections, mostly preserved on the reddish silt- to fine-grained rippled sandstone
459 bed tops. Conversely, the deposits of both the underlying Sunjiagou Formation and the
460 overlying Heshanggou Formation show rich bioturbation, but no MISS. Meanwhile, wrinkle
461 structures were widely found in the Liujiagou Formation in adjoining areas, and show similar
462 characteristics of spatial and temporal distribution (Chu et al., 2015). Similarly, microbial
463 mat-related biosedimentary structures were reported in the red beds of a Lower Triassic
464 siliciclastic playa environment from the central basin of the Middle Buntsandstein
465 (Wehrmann and Gerdes, 2012), as well as microbialites and oolites from the Buntsandstein
466 Group in Germany, although its depositional environment is still controversial (Paul and
467 Peryt, 2000; Weidlich, 2007).
468 Palaeoenvironmental conditions such as water depth, exposure and hydrodynamic
469 energy, control the distribution of MISS within these facies. In fact, specific environmental
470 conditions must exist to allow the corresponding MISS to form and be preserved in the rock
471 record. These conditions provide the habitat for thriving microbial ecosystems to develop and
472 offered long-term preservation potential (Hagadorn and Bottjer, 1997; Noffke et al., 2002;
473 Pruss et al., 2004). In the studied sections, the OES and wrinkle structures are found on
474 sandstone bed tops, which are inferred to have been deposited in storm-dominated or
475 storm-influenced siliciclastic settings from the presence of hummocky cross-stratification and

476 flat-pebble conglomerates (Fig. 12; Myrow et al., 2004; Morsilli and Pomar, 2012).
477 Storm-dominated siliciclastic settings are considered to be appropriate settings for mat growth
478 features where hydrodynamic flow is sufficient to sweep mud from mat surfaces but
479 insufficient to erode biostabilized laminae, so that a microbial-mat-colonized surface trapped
480 and bound the clean, fine-grained, translucent quartz grains (Noffke et al., 2002; Pruss et al.,
481 2004; Schieber et al., 2007).

482 In addition, for the beds that developed synaeresis shrinkage sand cracks,
483 short-wavelength ($\lambda < 50$ mm) and symmetrical ripples are common, and shrinkage sand
484 cracks are sometimes parallel to ripple troughs or crests (Fig. 2F). These ripples typically
485 have parallel and straight ripple crests and consistent crest orientations from bed to bed (Fig.
486 2F), indicating deposition in very shallow water across large areas. Meanwhile, the
487 fine-grained sandstone or siltstone beds commonly contain multiple generations of sand-filled
488 polygonal desiccation cracks, indicating periodic exposure (Fig. 10H). So, the occurrences of
489 synaeresis cracks and desiccation cracks, coupled with short-wavelength and symmetrical
490 ripples, indicate alternations between subaqueous and subaerial conditions, and deposition in
491 very shallow water.

492

493 **6.3. Implication for the post-extinction terrestrial ecosystems and the Early Triassic**
494 **biotic recovery**

495 Blooms of microbial communities in the aftermath of the PTME have been reported
496 worldwide from marine Lower Triassic successions, suggesting that microbial buildups and
497 mats dominated the seabed, preserved in the form of microbialites and wrinkle structures
498 (Kershaw et al., 1999; Pruss et al., 2004, 2006; Mata and Bottjer, 2009). For terrestrial
499 deposition during the post-extinction interval, MISS-related microbial mats were observed in
500 the Liujiagou Formation of North China and the Detfurth Formation of the Germanic Basin

501 (this study; Wehrmann and Gerdes, 2012; Tu et al., 2016), which might imply that microbial
502 communities proliferated both in the sea and on land through most of the Early Triassic.
503 Furthermore, records of terrestrial MISS and microbial organics also indicate extreme
504 environmental stresses following the PTME.

505 In particular, the detrimental effects of increased temperature and climatic drying,
506 presumably caused/exacerbated the extinction of terrestrial organisms (Benton and Newell,
507 2014), but provided the habitat for thriving microbial communities and favourable conditions
508 for MISS formation. The degradation of terrestrial ecosystems and turnover from an ever-wet
509 to a progressively drier and hotter climate immediately after the PTME were observed from
510 sedimentological studies in North China, and this promoted the widespread formation of
511 MISS. Furthermore, abnormal hydrochemical and physical environments may also have been
512 responsible for the low-level of bioturbation and flourishing of MISS in the aftermath of the
513 PTME, such as nutrient enrichment associated with enhanced nutrient input, decreased
514 solubility of oxygen associated with reduced atmospheric oxygen content and elevated
515 temperature, strong water energy, and geochemical anomalies associated with the climate
516 turnover (Berner et al., 2007; Algeo and Twitchett, 2010; Sun et al., 2012; Chu et al., 2015).

517 In the studied sections, MISS were limited in the lower to middle parts of the Liiujiagou
518 Formation and not observed yet in its upper part. This phenomenon is also reinforced by our
519 observations of the other sections in Henan, Shanxi and Shaanxi provinces. The investigation
520 of fossils and bioturbation index for these sections in North China demonstrated that the
521 absence of metazoans and decreased bioturbation intensity happened immediately after the
522 severe mass extinction, and only very rare trace fossils occurred in the lower to middle parts
523 of the Liujiagou Formation (Chu et al., 2015). In the upper part of the Liujiagou Formation,
524 MISS disappeared and burrows and surface traces discontinuously appeared, but significantly
525 were not recovered to the pre-extinction level of bioturbation intensity. Furthermore, the

526 overlying Heshanggou Formation shows diverse ichnofossils and rich bioturbation, with a
527 measured bioturbation index up to 5 (Fig. 13). So, the disappearance of MISS associated with
528 growing bioturbation in the upper part of the Liujiagou Formation and the Heshanggou
529 Formation might indicate an improved terrestrial ecosystem and the prologue of the Triassic
530 biotic recovery. However, the timing and pattern of the recovery of Early Triassic terrestrial
531 ecosystems and correlation between marine and terrestrial settings requires further
532 geobiological and geochemical studies, as well as high-precision isotopic dating, especially
533 for the terrestrial successions.
534
535 **7. Conclusions**
536 Five different kinds of MISS or sedimentary surface textures were recognized through
537 studies of morphology and microscopic characteristics. The microscopic features and SEM
538 images showing the presence of crinkly, dark and opaque clay laminae and floating quartz
539 grains, suggest that the microbial mats trapped sand grains from the surrounding environment
540 (Hagadorn and Bottjer, 1997). The depositional environments studied here demonstrate that
541 microbial communities in the lakes of the Liujiagou Formation were adapted not only to
542 periodically desiccated conditions, but also storm-dominated palaeoenvironments, which
543 provided the habitat for thriving microbial ecosystem development and offered long term
544 preservation potential.
545 The Sunjiagou Formation records the turnover of sedimentary systems and climate, and it
546 also records the terrestrial PTME in North China. Following the mass extinction, MISS
547 became much more common and widespread, which suggests that the mass extinction
548 provided favourable environmental and biological conditions for development of MISS in
549 terrestrial ecosystems, such as low-level bioturbation, decreased grazing pressure, and
550 enhanced nutrient input associated with the increased temperature and climatic drying. In

particular, the essential factor affecting the presence of MISS is the amount and level of bioturbation. However, a biotic crisis should not be considered as the only condition necessary for the formation of MISS. A full understanding of how MISS form in space and time will require a worldwide survey of original observations from various geological records and a comprehensive explanation should be addressed using large datatsets and empirical experimental modelling (e.g. Noffke and Awramik, 2013; Thomas et al., 2013; Mariotti et al., 2014; Davies et al., 2016). In addition, we propose that the disappearance of MISS coupled with growing bioturbation might indicate an improved terrestrial ecosystem and represent the prologue of the Triassic biotic recovery since the deposition of the Heshanggou Formation.

Acknowledgments

We thank Xincheng Qiu, Kaixuan Ji, and Wenchao Shu for help with sampling from the studied section. Hao Yang and Ruiwen Zong are thanked for assistance with obtaining SEM and microscope images at the State Key Laboratory of Biogeology and Environmental Geology, China University of Geosciences (Wuhan). Daoliang Chu thanks Zhongqiang Chen, Alexander Liu and Qingyu Ma for insightful discussions. Steve Zhang is thanked for revising the English of the manuscript draft. The authors are grateful to Sara Pruss, the anonymous reviewer and guest editor Zhong-Qiang Chen for their critical comments and constructive suggestions, which have greatly improved the quality of the paper. This study was supported by the National Natural Science Foundation of China (41272372, 41530104, 41402302), the 111 Project (B08030). It is a contribution to IGCP 630.

References

Abdolmaleki, J., Tavakoli, V., 2016. Anachronistic facies in the early Triassic successions of the Persian Gulf and its palaeoenvironmental reconstruction. Palaeogeography,

576 Palaeoclimatology, Palaeoecology 446, 213–224.
577 Algeo, T.J., Twitchett, R.J., 2010. Anomalous Early Triassic sediment fluxes due to elevated
578 weathering rates and their biological consequences. Geology 38, 1023–1026.
579 Algeo, T.J., Chen, Z. Q., Fraiser, M. L., Twitchett, R.J., 2011. Terrestrial-marine
580 teleconnections in the collapse and rebuilding of Early Triassic marine ecosystems.
581 Palaeogeography, Palaeoclimatology, Palaeoecology 308, 1–11.
582 Alroy, J., et al., 2008. Phanerozoic trends in the global diversity of marine invertebrates.
583 Science 321, 97–100.
584 Arche, A., Lopez-Gomez, J., 2005. Sudden changes in fluvial style across the
585 Permian-Triassic boundary in the eastern Iberian Ranges, Spain: analysis of possible
586 causes. Palaeogeography, Palaeoclimatology, Palaeoecology 229, 104–126.
587 Banerjee, S., Jeevankumar, S., 2005. Microbially originated wrinkle structures on sandstone
588 and their stratigraphic context: Palaeoproterozoic Koldaha Shale, central India.
589 Sedimentary Geology 176, 211–224.
590 Banerjee, S., Sarkar, S., Eriksson, P.G., Samanta, P., 2010. Microbially related structures in
591 siliciclastic sediment resembling Ediacaran fossils: examples from India, ancient and
592 modern. In: Seckbach, J., Oren, A. (Eds.), Microbial Mats: Modern and Ancient
593 Microorganisms in Stratified Systems. Springer-Verlag, Berlin, pp. 111 –129.
594 Baud, A., Richoz, S., Pruss, S., 2007. The Lower Triassic anachronistic carbonate facies in
595 space and time. Global and Planetary Change 55, 81 –89
596 Benton, M.J., 2015. When Life Nearly Died: The Greatest Mass Extinction of All Time,
597 second edition. Thames & Hudson, London, 352p.
598 Benton, M.J., Newell, A.J., 2014. Impacts of global warming on Permo-Triassic terrestrial
599 ecosystems. Gondwana Research 25, 1308–1337.
600 Benton, M.J., 2016. The Chinese pareiasaurs. Zoological Journal of the Linnean Society, in

press.

Berner, R.A., VandenBrooks, J.M., Ward, P.D., 2007. Oxygen and evolution. Science 316, 557–558.

Botha, J., Smith, R.M.H., 2006. Rapid vertebrate recuperation in the Karoo Basin of South Africa following the End-Permian extinction. Journal of African Earth Sciences 45, 502–514.

Bottjer, D., Hagadorn, J.W., 2007. Mat growth features. In: Schieber, J., Bose, P.K., Eriksson, P.G., Banerjee, S., Sarkar, S., Altermann, W., Catuneau, O. (Eds.), Atlas of Microbial Mat Features Preserved Within the Siliciclastic Rock Record, Atlases in Geosciences. Elsevier, Amsterdam, 53–71.

Buatois, L.A., Netto, R.G., Mángano, M.G., Carmona, N.B., 2013. Global deglaciation and the re-appearance of microbial matground-dominated ecosystems in the late Paleozoic of Gondwana. Geobiology 11, 307–317.

Cascales-Miñana, B., Cleal, C.J., 2014. The plant fossil record reflects just two great extinction events. Terra Nova 26, 195–200.

Cascales-Miñana, B., Diez, J.B., Gerrienne, P., Cleal, C.J., 2015. A palaeobotanical perspective on the great end-Permian biotic crisis. Historical Biology, doi:10.1080/08912963.2015.1103237.

Callow, R.H.T., Battison, L., Brasier, M.D., 2011. Diverse microbially induced sedimentary structures from 1 Ga lakes of the Diabaig Formation, Torridon Group, northwest Scotland. Sedimentary Geology 239, 117–128.

Calner, M., 2005. A Late Silurian extinction event and anachronistic period. Geology 33, 305–308.

Carmona, N.B., Ponce, J.J., Wetzel, A., Bournod, C.N., Cuadrado, D.G., 2012. Microbially induced sedimentary structures in Neogene tidal flats from Argentina:

626 paleoenvironmental, stratigraphic and taphonomic implications. Palaeogeography,
627 Palaeoclimatology, Palaeoecology 353–355, 1–9.
628 Chen, Z.Q., Benton, M.J., 2012. The timing and pattern of biotic recovery following the
629 end-Permian mass extinction. Nature Geoscience 5, 375–383.
630 Chen, Z.Q., Wang, Y.B., Kershaw, S., Luo, M., Yang, H., Zhao, L.S., Fang, Y.H., Chen, J.B.,
631 Yang, L., Zhang, L., 2014. Early Triassic stromatolites in a siliciclastic nearshore setting
632 in northern Perth Basin, Western Australia: geobiologic features and implications for
633 post-extinction microbial proliferation. Global and Planetary Change 121, 89 –100.
634 Chu, D.L., Tong, J.N., Song, H.J., Benton, M.J., Bottjer, D.J., Song, H.Y., Tian, L., 2015.
635 Early Triassic wrinkle structures on land: stressed environments and oases for life.
636 Scientific Reports 5, e10109, doi: 10.1038/srep10109.
637 Chu, D.L., Yu, J.X., Tong, J.N., Benton, M.J., Song, H.J., Huang, Y.F., Song, T., Tian, L., in
638 review. Biostratigraphic correlation and mass extinction during the Permian-Triassic
639 transition in terrestrial-marine siliciclastic settings of South China. Global and Planetary
640 Change.
641 Dai, H., Xing, L. D., Marty, D., Zhang, J. P., Persons, W. S. I. V., Hu, H. Q., Wang, F.P.,
642 2015. Microbially-induced sedimentary wrinkle structures and possible impact of
643 microbial mats for the enhanced preservation of dinosaur tracks from the Lower
644 Cretaceous Jiaguan Formation near Qijiang (Chongqing, China). Cretaceous Research,
645 53, 98–109.
646 Davies, N.S., Liu, A.G., Gibling, M.R, Miller, R.F., 2016. Resolving MISS conceptions and
647 misconceptions: A geological approach to sedimentary surface textures generated by
648 microbial and abiotic processes. Earth-Science Reviews, in press, doi:
649 10.1016/j.earscirev.2016.01.005.
650 Endo, R., 1933. *Manchuriophycus* nov. gen. from a Sinian Formation of South Manchuria.

651 Japanese Journal of Geology and Geography 11, 43–48.
652 Eriksson, P.G., Schieber, J., Bouougri, E., Gerdes, G., Porada, H., Banerjee, S., Bose, P.K.,
653 Sarkar, S., 2007. Classification of structures left by microbial mats in their host
654 sediments. In: Schieber, J., Bose, P.K., Eriksson, P.G., Banerjee, S., Sarkar, S.,
655 Altermann, W., Catuneau, O. (Eds.), Atlas of Microbial Mat Features Preserved Within
656 the Siliciclastic Rock Record, Atlases in Geosciences. Elsevier, Amsterdam, 39–52.
657 Erwin, D.H., 1993. The great Paleozoic crisis: life and death in the Permian. Columbia
658 University Press, New York, 327 pp.
659 Gao, K.Q., 1983. A new pareiasaur from Liulin, Shanxi. Vertebrata PalAsiatica 2, 193–203
660 (in Chinese with English summary).
661 Gao, K.Q., 1989. Pareiasaurs from the Upper Permian of north China. Canadian Journal of
662 Earth Sciences 26, 1234–1240.
663 Gastaldo, R.A., Kamo, S.L., Neveling, J., Geissman, J.W., Bamford, M., Looy, C.V., 2015. Is
664 the vertebrate-defined Permian-Triassic boundary in the Karoo Basin, South Africa, the
665 terrestrial expression of the end-Permian marine event? Geology 43, 939–942.
666 Gehling, J. G., 1999. Microbial mats in terminal Proterozoic siliciclastics: Ediacaran death
667 masks. Palaios 14, 40–57.
668 Gehling, J.G., 2000. Environmental interpretation and a sequence stratigraphic framework for
669 the terminal Proterozoic Ediacara Member within the Rawnsley Quartzite, South
670 Australia. Precambrian Research 100, 65–95.
671 Gerdes, G., Klenke, Th., Noffke, N., 2000. Microbial signatures in peritidal siliciclastic
672 sediments: a catalogue. Sedimentology 47, 279–308.
673 Grauvogel-Stamm, L., Ash, S.R., 2005. Recovery of the Triassic land flora from the
674 end-Permian life crisis. Comptes Rendus Palevol l4, 593–608.
675 Grotzinger, J.P., Knoll, A.H., 1995. Anomalous carbonate precipitates: Is the Precambrian the

676 key to the Permian? Palaios 10, 578–596.
677 Hagadorn, J.W., Bottjer, D.J., 1997. Wrinkle structures: microbially mediated sedimentary
678 structures common in subtidal siliciclastic settings at the Proterozoic–Phanerozoic
679 transition. Geology 25, 1047–1050.
680 Hagadorn, J.W., Bottjer, D.J., 1999. Restriction of a late Neoproterozoic biotope; suspect-
681 microbial structures and trace fossils at the Vendian–Cambrian transition. Palaios 14,
682 73–85.
683 Hermann, E., Hochuli, P.A., Bucher, H., Bruhwiler, T., Hautmann, M., Ware, D., Roohi, G.,
684 2011. Terrestrial ecosystems on North Gondwana following the end-Permian mass
685 extinction. Gondwana Research 20, 630–637.
686 Hofmann, H.J., 1967. Precambrian fossils (?) near Elliot lake, Ontario. Science 156, 500–504.
687 Hou, J.P., Ouyang, S., 2000. Palynoflora from the Sunjiagou Formation in Liulin County,
688 Shanxi Province. Acta Palaeontoloica Sinica 39, 356–368.
689 Ibarra, Y., Corsetti, F.A., Greene, S.E., Bottjer, D.J., 2016. A microbial carbonate response in
690 synchrony with the end-Triassic mass extinction across the SW UK. Scientific Reports 6,
691 e19808, doi: 10.1038/srep19808.
692 Kershaw, S., Zhang, J., Lan, G., 1999. A microbialite carbonate crust at the Permian–Triassic
693 boundary in south China, and its palaeoenvironmental significance. Palaeogeography,
694 Palaeoclimatology, Palaeoecology 146, 1–18.
695 Knaust, D., 2010. The end-Permian mass extinction and its aftermath on an equatorial
696 carbonate platform: insights from ichnology. Terra Nova 22, 195–202.
697 Koehn, D., Bons, P., Montenari, M., Seilacher, A., 2014. The elastic age: rise and fall of
698 Precambrian biomat communities. EGU Geophysical Research Abstracts 16,
699 EGU2014-13793.
700 Lan, Z.W., Chen, Z.Q., 2012. Exceptionally preserved microbially induced sedimentary

701 structures from the Ediacaran post-glacial successions in the Kimberley region,
702 northwestern Australia. Precambrian Research 200–203, 1–25.
703 Lan, Z.W., Chen, Z.Q., 2013. Proliferation of MISS-forming microbial mats after the late
704 Neoproterozoic glaciations: Evidence from the Kimberley region, NW Australia.
705 Precambrian Research 224, 529–550.
706 Lan, Z.W., 2015. Paleoproterozoic microbially induced sedimentary structures from lagoonal
707 depositional settings in northern China. Sedimentary Geology 328, 87–95.
708 Lehrmann, D.J., 1999. Early Triassic calcimicrobial mounds and biostromes of the
709 Nanpanjiang Basin, south China. Geology 27, 359–362.
710 Li, X.W., Liu, J., 2013. New specimens of pareiasaurs from the Upper Permian Sunjiagou
711 Formation of Liulin, Shanxi and their implications for the taxonomy of Chinese
712 pareiasaurs. Vertebrata PalAsiatica 51, 199–204.
713 Liu, F., Zhu, H.C., Ouyang, S., 2015. Late Pennsylvanian to Wuchiapingian
714 palynostratigraphy of the Baode section in the Ordos Basin, North China. Journal of
715 Asian Earth Sciences 111, 528–552.
716 Looy, C.V., Brugman, W.A., Dilcher, D.L., Visscher, H., 1999. The delayed resurgence of
717 equatorial forests after the Permian-Triassic ecologic crisis. Proceedings of the National
718 Academy of Sciences, U.S.A. 96, 13857–13862.
719 Looy, C.V., Twitchett, R.J., Dilcher, D.L., Van Konijnenburg-Van Cittert, J.H., Visscher, H.,
720 2001. Life in the end-Permian dead zone. Proceedings of the National Academy of
721 Sciences, U.S.A. 98, 7879–7883.
722 Mata, S.A., Bottjer, D.J., 2009. The paleoenvironmental distribution of Phanerozoic wrinkle
723 structures. Earth Science-Reviews 96, 181–195.
724 Mariotti, G., Pruss, S. B., Perron, J. T., Bosak, T., 2014, Microbial shaping of sedimentary
725 wrinkle structures. Nature Geoscience 7, 736–40.

726 McLoughlin, N., Wilson, L.A., Brasier, M.D., 2008. Growth of synthetic stromatolites and
727 wrinkle structures in the absence of microbes — implications for the early fossil record.
728 Geobiology 6, 95–105.
729 Metcalfe, I., Crowley, J.L., Nicoll, R.S., Schmitz, M., 2015. High-precision U-Pb CA-TIMS
730 calibration of Middle Permian to Lower Triassic sequences, mass extinction and extreme
731 climate-change in eastern Australian Gondwana. Gondwana Research 28, 61–81.
732 Meyer, M., Xiao, S., Gill, B.C., Schiffbauer, J.D., Chen, Z., Zhou, C., Yuan, X., 2014.
733 Interactions between Ediacaran animals and microbial mats: insights from *Lamonte*
734 *trevallis*, a new trace fossil from the Dengying Formation of South China.
735 Palaeogeography, Palaeoclimatology, Palaeoecology 396, 62–74.
736 Miall, A.D., Jones, B.G., 2003. Fluvial architecture of the Hawkesbury sandstone (Triassic),
737 near Sydney, Australia. Journal of Sedimentary Research 73, 531–545.
738 Michaelsen, P., 2002. Mass extinction of peat-forming plants and the effect on fluvial styles
739 across the Permian-Triassic boundary, northern Bowen Basin, Australia.
740 Palaeogeography, Palaeoclimatology, Palaeoecology 179, 173–188.
741 Miller, M. F., Smail, S. E., 1997. A semiquantitative field method for evaluating bioturbation
742 on bedding planes. Palaios 12, 391–396.
743 Morsilli, M., Pomar, L., 2012. Internal waves vs. surface storm waves: a review on the origin
744 of hummocky cross-stratification. Terra Nova 24, 273–282.
745 Myrow, P.M., Tice, L., Archuleta, B., Clark, B., Taylor, J., Ripperdan, R.L., 2004.
746 Flat-pebble conglomerate; its multiple origins and relationship to metre-scale
747 depositional cycles. Sedimentology 51, 973–996.
748 Newell, A. J., Tverdokhlebov, V. P., Benton, M. J., 1999. Interplay of tectonics and climate
749 on a transverse flvial system, Upper Permian, Southern Uralian Foreland Basin, Russia.
750 Sedimentary Geology 127, 11–29.

751 Noffke, N., Gerdes, G., Klenke, T., Krumbein, W.E., 2001. Microbially induced sedimentary
752 structures—a new category within the classification of primary sedimentary structures.
753 Journal of Sedimentary Research 71, 649–656.
754 Noffke, N., Knoll, A .H., Grotzinger, J., 2002. Sedimentary controls on the formation and
755 preservation of microbial mats in siliciclastic deposits: a case study from the upper
756 Neoproterozoic Nama Group, Namibia. Palaios 17, 1–14.
757 Noffke, N., Hazen, R.M., Nhleko, N., 2003. Earth's earliest microbial mats in a siliciclastic
758 marine environment (Mozaan Group, 2.9 Ga, South Africa). Geology 31, 673– 676.
759 Noffke, N., Hazen, R.M., Erik sson, K., Simpson, E., 2006. A new window into early life:
760 microbial mats in a siliciclastic early Archean tidal flat (3.2 Ga Moodies Group, South
761 Africa). Geology 34, 253–256.
762 Noffke, N., Paterson, D., 2008. Microbial interactions with physical sediment dynamics, and
763 their significance for the interpretation of Earth's biological history. Geobiology 6, 1–4.
764 Noffke, N., 2009. The criteria for the biogeneicity of microbially induced sedimentary
765 structures (MISS) in Archean and younger, sandy deposits. Earth-Science Reviews 96,
766 173–180.
767 Noffke, N., 2010. Geobiology: Microbial Mats in Sandy Deposits from the Archean Era to
768 Today. Heidelberg, Springer, 196 p.
769 Noffke, N., and Chafetz, H., 2012. Microbial Mats in Siliciclastic Depositional Systems
770 through Time: SEPM (Society for Sedimentary Geology) Special Publication 101, 200 p.
771 Noffke, N., Awramik, S.M., 2013. Stromatolites and MISS—differences between relatives.
772 GSA Today 23, doi: 10.1130/GSATG187A.1.
773 Parizot, M., Eriksson, P.G., Aifa, T., Sarkar, S., Banerjee, S., Catuneanu, O., Altermann, W.,
774 Bumby, A.J., Bordy, E.M., van Rooy, J.L., Boshoff, A.J., 2005. Suspected microbial
775 mat-related crack-like sedimentary structures in the Palaeoproterozoic Magaliesberg

776 Formation sandstones, South Africa. Precambrian Research 138, 274–296.
777 Paul, J., Peryt, T.M., 2000. Kalkowsky's stromatolites revisited (Lower Triassic
778 Buntsandstein, Harz Mountains, Germany). Palaeogeography, Palaeoclimatology,
779 Palaeoecology 161, 435–458.
780 Peterffy, O., Calner, M., Vajda, V., 2016. Early Jurassic microbial mats-a potential response
781 to reduced biotic activity in the aftermath of the end-Triassic mass extinction event.
782 Palaeogeography, Palaeoclimatology, Palaeoecology, in press.
783 Pflüger, F., 1999. Matground structures and redox facies. Palaios 14, 25–39.
784 Plummer, P.S., Gostin, V.A., 1981. Shrinkage cracks: desiccation or synaeresis? Journal of
785 Sedimentary Research 51, 1147–1156.
786 Prave, A.R., 2002. Life on land in the Proterozoic: Evidence from the Torridonian rocks of
787 northwest Scotland. Geology 30, 811–814.
788 Pruss, S.B., Fraiser, M.L., Bottjer, D.J., 2004. The global proliferation of Early Triassic
789 wrinkle structures: implications for environmental stress following the end-Permian mass
790 extinction. Geology 32, 461– 464.
791 Pruss, S.B., Bottjer, D.J., 2004. Late Early Triassic microbial reefs of the western United
792 States: a description and model for their deposition in the aftermath of the end-Permian
793 mass extinction. Palaeogeography, Palaeoclimatology, Palaeoecology 211, 127– 137.
794 Pruss, S.B., Corsetti, F.A., Bottjer, D.J., 2005. The unusual sedimentary rock record of the
795 Early Triassic: a case study from the southwestern United States. Palaeogeography,
796 Palaeoclimatology, Palaeoecology 222, 33–52.
797 Pruss, S.B., Bottjer, D.J., Corsetti, F.A., Baud, A., 2006. A global marine sedimentary
798 response to the end-Permian mass extinction: examples from southern Turkey and the
799 western United States. Earth-Science Reviews 78, 193–206.
800 Porada, H., Bouougri, E. H., 2007. Wrinkle structures-a critical review. Earth-Science

Reviews 81, 199–215.

Rakociński, M., Racki, G., 2016. Microbialites in the shallow-water marine environments of the Holy Cross Mountains (Poland) in the aftermath of the Frasnian-Famennian biotic crisis. Global and Planetary Change 136, 30–40.

Rees, P.M., 2002. Land-plant diversity and the end-Permian mass extinction. Geology 30, 827–830.

Retallack, G.J., 1995. Permian-Triassic life crisis on land. Science 267, 77–80.

Retallack, G.J., Veevers, J.J., Morante, R., 1996. Global coal gap between Permian-Triassic extinction and Middle Triassic recovery of peat-forming plants. Geological Society of America Bulletin 108, 195–207.

Retallack, G.J., 2005. Earliest Triassic claystone breccias and soil-erosion crisis. Journal of Sedimentary Research 75, 679–695.

Retallack, G.J., Sheldon, N.D., Carr, P.F., Fanning, M., Thompson, C.A., Williams, M.L., Jones, B.G., Hutton, A., 2011. Multiple Early Triassic greenhouse crises impeded recovery from Late Permian mass extinction. Palaeogeography, Palaeoclimatology, Palaeoecology 308, 233–251.

Retallack, G.J., 2013. Permian and Triassic greenhouse crises. Gondwana Research 24, 90–103.

Schieber, J., Bose, P.K., Eriksson, P.G., Banerjee, S., Sarkar, S., Alterman, W., Catuneanu, O., 2007. Atlas of Microbial Mat Features Preserved within the Siliciclastic Rock Record. Atlases in Geosciences, Amsterdam, Elsevier, 311 p.

Schneebeli-Hermann, E., Kürschner, W.M., Kerp, H., Bomfleur, B., Hochuli, P.A., Bucher, H., Ware, D., Roohi, G., 2015. Vegetation history across the Permian-Triassic boundary in Pakistan (Amb section, Salt Range). Gondwana Research 27, 911–924.

Schubert, J.K., Bottjer, D.J., 1992. Early Triassic stromatolites as post-mass extinction

826 disaster forms. Geology 20, 883–886.
827 Sepkoski, J.J., Bambach, R.K., Droser, M.L., 1991. Secular changes in Phanerozoic event
828 bedding and the biological imprint. In: Einsele, G., Ricken, W., Seilacher, A. (Eds.),
829 Cycles and Events in Stratigraphy. Springer-Verlag, Berlin, pp. 298–312.
830 Sheehan, P.M., Harris, M.T., 2004. Microbialite resurgence after the Late Ordovician
831 extinction. Nature 430, 75–77.
832 Shen, S.Z., Crowley, J.L., Wang, Y., Bowring, S.A., Erwin, D.H., Sadler, P.M., Cao, C.Q.,
833 Rothman, D.H., Henderson, C.M., Ramezani, J., Zhang, H., Shen, Y., Wang, X.D.,
834 Wang, W., Mu, L., Li, W.Z., Tang, Y.G., Liu, X.L., Liu, L.J., Zeng, Y., Jiang, Y.F., Jin,
835 Y.G., 2011. Calibrating the end-Permian mass extinction. Science 334, 1367–1372.
836 Simpson, E.L., Heness, E.A., Bumby, A.J., Eriksson, P.G., Eriksson, K.A., Hilbert-Wolf,
837 H.L., Linnevelt, S., Fitzgerald Malenda, H., Modungwa, T., Okafor, O.J., 2013. 2.0 Ga
838 continental microbial diversity in a paleodesert setting. Precambrian Research 237,
839 36–50.
840 Smith, R.M.H., Botha-Brink, J., 2014. Anatomy of a mass extinction: sedimentological and
841 taphonomic evidence for drought-induced die-offs at the Permo-Triassic boundary in the
842 main Karoo Basin, South Africa. Palaeogeography, Palaeoclimatology, Palaeoecology
843 396, 99–118.
844 Song, H.J., Wignall, P.B., Tong, J.N, Yin, H.F., 2013. Two pulses of extinction during the
845 Permian-Triassic crisis. Nature Geoscience 6, 52–56.
846 Song H.J., Wignall, P.B., Tong J.N., Song H.Y., Chen J., Chu D.L., Tian L., Luo M., Zong
847 K.Q., Chen Y.L., Lai X.L., Zhang K.X., Wang H.M., 2015. Integrated Sr isotope
848 variations and global environmental changes through the Late Permian to early Late
849 Triassic. Earth and Planetary Science Letters 424, 140-147.
850 Stevens, L.G., Hilton, J., Bond, D.P.G., Glasspool, I.J., Jardine, P.E., 2011. Radiation and

851 extinction patterns in Permian floras from North China as indicators for environmental
852 and climate change. Journal of the Geological Society 168, 607–619.
853 Strother, P.K., Wellman, C.H., 2015. Palaeoecology of a billion-year-old non-marine
854 cyanobacterium from the Torridon Group and Nonesuch Formation. Palaeontology 59,
855 89–108.
856 Sun, Y.D., Joachimski, M.M., Wignall, P.B., Yan, C.B., Chen, Y.L., Jiang, H.S., Wang, L.N.,
857 Lai, X.L., 2012. Lethally hot temperatures during the early Triassic greenhouse. Science
858 338, 366–370.
859 Taylor, G.K., Tucker, C., Twitchett, R J., Kearsey, T., Benton, M.J., Newell, A.J., Surkov,
860 M.V., Tverdokhlebov, V.P., 2009. Magnetostratigraphy of Permian/ Triassic boundary
861 sequences in the Cis-Urals, Russia: No evidence for a major temporal hiatus. Earth and
862 Planetary Science Letters 281,36–47.
863 Thomas, K., Erminghaus, S., Porada, H., Gohering, L., 2013. Formation of kinneyia via
864 shear-induced instabilities in microbial mats. Philosophical Transactions of the Royal
865 Society Association 371, 20120362, doi: 10.1098/rsta.2012.0362.
866 Tu, C.Y., Chen, Z.Q., Retallack, G.J., Huang, Y.G., Fang, Y.H., 2016. Proliferation of
867 MISS-related microbial mats following the end-Permian mass extinction in terrestrial
868 ecosystems: Evidence from the Lower Triassic of the Yiyang area, Henan Province,
869 North China. Sedimentary Geology 333, 50–69.
870 Twitchett, R.J., Looy, C.V., Morante, R., Visscher, H., Wignall, P.B., 2001. Rapid and
871 synchronous collapse of marine and terrestrial ecosystems during the end-Permian biotic
872 crisis. Geology 29, 351–354.
873 Veevers, J. J., Conaghan, P. J., and Shaw, S. E., 1994. Turning point in Pangean
874 environmental history of the Permo-Triassic (P-Tr) boundary. In Klein, G. de V., ed.,
875 Pangea: Paleoclimate, tectonics, and sedimentation during accretion, zenith and breakup

876 of a supercontinent: Geological Society of America Special Paper 288, 187–196.
877 Wang, Z.Q., Wang, L.X., 1982. A new species of the lycopsid *Pleuromeia* from the Early
878 Triassic of Shanxi, China, and its ecology. Palaeontology 25, 215–225.
879 Wang, Z.Q., Wang, L.X., 1986. Late Permian fossil plants from the lower part of the
880 Shiqianfeng (Shihchienfeng) group in North China. Bulletin Tianjin Institute Geology
881 and Mineral Resources15, 1–80 (in Chinese with English abstract).
882 Wang, Z.Q., 1996. Recovery of vegetation from the terminal Permian mass extinction in
883 North China. Review of Palaeobotany and Palynology 91, 121–142.
884 Ward, P.D., Montgomery, D.R., Smith, R., 2000. Altered river morphology in South Africa
885 related to the Permian-Triassic extinction. Science 289, 1740–1743.
886 Ward, P.D., Botha, J., Buick, R., De Kock, M.O., Erwin, D.H., Garrison, G.H., Kirschvink,
887 J.L., Smith, R., 2005. Abrupt and gradual extinction among Late Permian land
888 vertebrates in the Karoo Basin, South Africa. Science 307, 709–714.
889 Wehrmann, A., Gerdes, G., Höfling, R., 2012. Microbial mats in a lower Triassic siliciclastic
890 playa environment (Middle Buntsandstein, North Sea). In: Noffke, N., Chafetz, H. (eds)
891 Microbial mats in siliciclastic depositional systems through time. SEPM Special
892 Publication 101, 177–190.
893 Weidlich, O., 2007. PTB mass extinction and earliest Triassic recovery overlooked? New
894 evidence for a marine origin of Lower Triassic mixed carbonate-siliciclastic sediments
895 (Rogenstein Member), Germany. Palaeogeography, Palaeoclimatology, Palaeoecology
896 252, 259–269.
897 Whalen, M.T., Day, J., Eberli, G.P., Homewood, P.W., 2002. Microbial carbonates as
898 indicators of environmental change and biotic crises in carbonate systems: Examples
899 from the Late Devonian, Alberta basin, Canada: Palaeogeography, Palaeoclimatology,
900 Palaeoecology 181, 127–151.

Wignall, P.B., Twitchett, R.J., 1999. Unusual intraclastic limestones in Lower Triassic carbonates and their bearing on the aftermath of the end-Permian mass extinction. Sedimentology 46, 303–316.

Wilmeth, D.T., Dornbos, S., Isbell, J.L., Czaja, A.D., 2014. Putative domal microbial structures in fluvial siliciclastic facies of the Mesoproterozoic (1.09 Ga) Copper Harbor Conglomerate, Upper Peninsula of Michigan, USA. Geobiology 12, 99–108.

Woods, A.D., Bottjer, D.J., Mutti, M., Morrison, J., 1999. Lower Triassic large sea-floor carbonate cements; their origin and a mechanism for the prolonged biotic recovery from the end-Permian mass extinction. Geology 27, 645– 648.

Xing, L.D., Lockley, M.G., Yang, G., Cao, J., McCrea, R.T., Klein, H., Zhang, J.P., Persons IV, W.S., Dai, H., 2016. A diversified vertebrate ichnite fauna from the Feitianshan Formation (Lower Cretaceous) of southwestern Sichuan, China. Cretaceous Research 57, 79–89.

Xu, L,, Li, X.W., Jia, S.H., Liu, J., 2015. The Jiyaun tetrapod fauna of the Upper Permian of China. New pareiasaur material and the reestablishment of Honania complicidentata. Acta Palaeontologica Polonica 60, 689–700.

Young, C.C., Yeh, H.K., 1983. On a new pareiasaur from the Upper Permian of Shansi, China. Vertebrata PalAsiatica 17, 195–214 (in Chinese with English abstract).

Yu, J.X., Broutin, J., Chen, Z.Q., Shi, X., Li, H., Chu, D.L., Huang, Q.S., 2015. Vegetation changeover across the Permian-Triassic Boundary in Southwest China. Extinction, survival, recovery and palaeoclimate: A critical review. Earth-Science Reviews 149, 202–224.

Zhang, H., Cao, C.Q., Liu, X.L., Mu, L., Zheng, Q.F., Liu, F., Xiang, L., Liu, L.J., Shen, S.Z., 2015. The terrestrial end-Permian mass extinction in South China. Palaeogeography, Palaeoclimatology, Palaeoecology 448, 108–124.

926 Zhang, H.Q., Liu, Y.h., Lin, D.C., 1987. The discovery of a plant fossil assemblage in the
927 Shiqianfeng Formation in Yiyang, Henan, and its significance. Regional Geology of
928 China 4, 383–384. (in Chinese with English abstract).
929 Zhang ,Y., Zheng, S.L., Naugolnykh, S.V., 2012. A new species of *Lepidopteris* discovered
930 from the Upper Permian of China with its stratigraphic and biologic implications.
931 Chinese Science Bulletin 57, 3603–3609.
932

933 **Figure captions**

934 **Fig. 1.** Investigated localities and columnar sections. (A) Sketch map of China, showing the
935 locations of Henan Province and Shanxi Province (grey shading). (B) Locations of the studied
936 sections. (C) Stratigraphic sections showing lithologies and distribution of MISS and fossils.
937 Abbreviations: Fm, Formation.

938

939 **Fig. 2.** Field photographs of the studied sections. (A) Field photograph showing the Dayulin
940 section and the boundary between the Sunjiagou and Liujiagou formations. (B) Field
941 photograph showing the Sunjiagou Formation in the Liulin section. (C) Field photograph
942 showing the Liujiagou Formation outcrop of the Liulin section along the eastern bank of the
943 Yellow River. (D) Sandstones of the Liujiagou Formation in the Liulin section containing
944 cross bedding and parallel bedding. (E) Brown-reddish fine-grained sandstones and siltstones
945 of the Liujiagou Formation. (F) Ripple marks of the Liujiagou Formation in the Dayulin
946 section, showing the short-wavelength and symmetrical ripples, the parallel and straight ripple
947 crests and consistent crest orientations from bed to bed. Lens cap diameter = 55 mm.

948

949 **Fig. 3.** Old elephant skin (OES) textures. (A) OES textures preserved on rippled sandstone
950 bed tops, collected from the middle part of the Liujiagou Formation in the Liulin section.
951 (B-D) Close-up of (A) showing OES textures are composed of convex epireliefs with
952 polygonal texture or elongate to elliptical bulges. (E) OES textures preserved on rippled
953 sandstone bed tops and confined to the crests of the ripples. (F) Close-up of (E) showing OES
954 textures are composed of convex epireliefs with polygonal texture. Coin diameter = 20 mm.

955

956 **Fig. 4.** Thin section photomicrographs of Figure 3A. (A–D) Photomicrographs showing the
957 presence of thin, wavy, crinkly and dark clay laminae on the bedding surface. (E) Thin section

of the dark clay laminae preserved within the sandstone of Fig. 3A, and showing the change in grain size between the upper and lower parts of the thin section.

Fig. 5. Photographs of wrinkle structures. (A) Cross cutting wrinkle structures collected from the lower part of the Liujiagou Formation in the Dayulin section. (B, C) Cross cutting wrinkle structures collected from the middle part of the Liujiagou Formation in the Liulin section. (D) Parallel wavy wrinkle structures collected from the lower part of the Liujiagou Formation in the Dayulin section, showing sinuously curved continuous wrinkles. (E, F) Parallel wavy wrinkle structures collected from the middle part of the Liujiagou Formation in the Liulin section, showing sinuously curved continuous crests and narrow troughs of the wrinkles.

Fig. 6. Details of wrinkle structures. **(**A, B) Vertical slab of a wrinkle structure cut perpendicular to the bedding surface along the black line in (A), showing the change in grain sizes. (C) Amalgamated thin section photomicrographs showing dark clay laminae and a change in grain size, corresponding to the area of the black box in (B). (D–E) Thin sections of the complete structure of the wrinkles of Fig. 5D. (F) Bulge-like wrinkle structures collected from the middle part of the Liujiagou Formation in the Liulin section. (G–I) Thin section of the wrinkle features in (F), showing the presence of thin, wavy, crinkly and dark clay laminae on the bedding surface.

Fig. 7. Details of bulge-like wrinkle structures and palimpsest structures. (A) Bulge-like wrinkle structures collected from the lower part of the Liujiagou Formation in the Dayulin section. (B) Close-up of (A), showing wrinkle features composed of elongate to subrounded bulges. (C) Palimpsest ripple structure preserved as two successive sets of ripples, collected from the middle part of Liujiagou Formation in the Liulin section. (D) Close-up of (C)

showing the diamond-like structures with subrounded and coalesced bulges or quasi-polygonal textures.

Fig. 8. Photographs of "*Manchuriophycus*" structures. (A, B) Sinuous cracks with positive patterns confined to troughs between ripples on the surfaces of sandstone beds, collected from the middle part of the Liujiagou Formation in the Dayulin section. (C, D) Sinuous cracks with negative patterns confined to ripple crests, collected from the lower part of the Liujiagou Formation in the Dayulin section. Lens cap diameter = 55 mm. (E, F) Photographs showing circular, sigmoidal and figure-8-shaped crack fills, collected from the middle part of the Liujiagou Formation in the Liulin section.

Fig. 9. Sand cracks preserved on sandstone bed tops of the middle part of the Liujiagou Formation in the Dayulin section, and thin section photomicrographs. (A) Pedate cracks. (B) Mesh-like cracks preserved as positive quasi-polygonal structures. (C, D) Spindle-shaped sand cracks confined to ripple crests, preserved as positive epireliefs, and developed on the wrinkle surface of sandstones. (E) Photomicrographs of the thin section in (D), showing the dark clay laminae preserved on the wrinkle surface.

Fig. 10. Plant fossils and trace fossils. (A–D) Photographs of plant fossils collected from the lower part of the Sunjiagou Formation in the Dayulin section, assigned to the genera *Taeniopteris*, *Ullmannia*, *Majonica* and *Lobatannularia*, respectively. (E) The last appearance of a coal bed/seam in the lower part of the Sunjiagou Formation in the Liulin section. (F) Abundant trace fossils preserved on a fine-grained sandstone bedding surface from the lower part of the Sunjiagou Formation. (G) Angular poorly sorted red mud rock clasts within sandstones of the Liujiagou Formation in the Dayulin section. (H) Desiccation cracks

preserved on a sandstone bedding surface of the Liujiagou Formation in the Dayulin section. Lens cap diameter = 55 mm.

Fig. 11. The distribution of bedding-plane bioturbation index (BPBI), plants, coal, tetrapods (pareiasaurs) and palynomorphs in the Sunjiagou Formation of the studied area, showing the Sunjiagou Formation spanning the PTME. The lithology is on the basis of the Dayulin section; the bioturbation index showing decreased bioturbation intensity in the upper part of Sunjiagou Formation and Liujiagou Formation; the extinction of plants occurred in the lower part of the Sunjiagou Formation in the Dayulin section (this study; Zhang et al., 1987), 1. *Pityospermum junduensis* Wang; 2. *Quadrocladus* cf. *orobiformis* (Schlotheim) Schweitzer; 3. *Pseudovoltzia* cf. *liebeana* (Geinitz) Florin; 4. *Pseudovoltzia* sp.; 5 *Sphenobaiera* sp.; 6. *Lobatannularia* sp.; 7. *Ullmannia bronni* Goeppert; 8. *Taeniopteris* sp.; the last occurrence of coal beds occurred in the lower part of the Sunjiagou Formation; the mass extinction of pareiasaurs occurred in the upper part of the Sunjiagou Formation (Benton, 2016); the first appearance of the Triassic-type *Lundbladispora-Taeniaesporites* palynomorph assemblage occurred in the upper part of the Sunjiagou Formation (Hou and Ouyang 2000). The upper part of the Sunjiagou Formation corresponds to the Permian-Triassic transitional beds. Abbreviations: Fm, Formation; Th, Thickness; BPBI, Bedding Plane Bioturbation Index (Miller and Smail, 1997).

Fig. 12. Sedimentary textures and structures. (A) Field photograph showing large-scale hummocky cross-stratification in the lower part of the Liujiagou Formation in the Dayulin section. (B) Field photograph showing small-scale hummocky cross-stratification in the middle part of the Liujiagou Formation in the Liulin section. (C) Conglomerates with lenticular, rounded and quasi-polygonal shapes. (D) Sandstone with interbed of flat-pebble

conglomerates, observed in the lower part of the Liujiagou Formation in the Dayulin section. Coin diameter = 20 mm.

Fig. 13. Burrows and surface traces from the upper part of Liujiagou Formation and Heshanggou Formation. (A) A surface assemblage of slender traces from the upper part of Liujiagou Formation. (B) Vertical burrows extend to a depth of 50–100 mm in the upper part of the Liujiagou Formation. (C) An assemblage of surface traces and burrows, assigned to *Planolites* and *Skolithos*, from the bottom of the Heshanggou Formation. (D, E) Limulid trackways preserved on bedding planes, from the lower part of the Heshanggou Formation. (F) A curved burrow with a maximum diameter of 25 mm, from the lower part of the Heshanggou Formation. (G) A dense assemblage of surface traces and burrows, assigned to *Planolites* and *Skolithos*, collected from the middle part of the Heshanggou Formation.

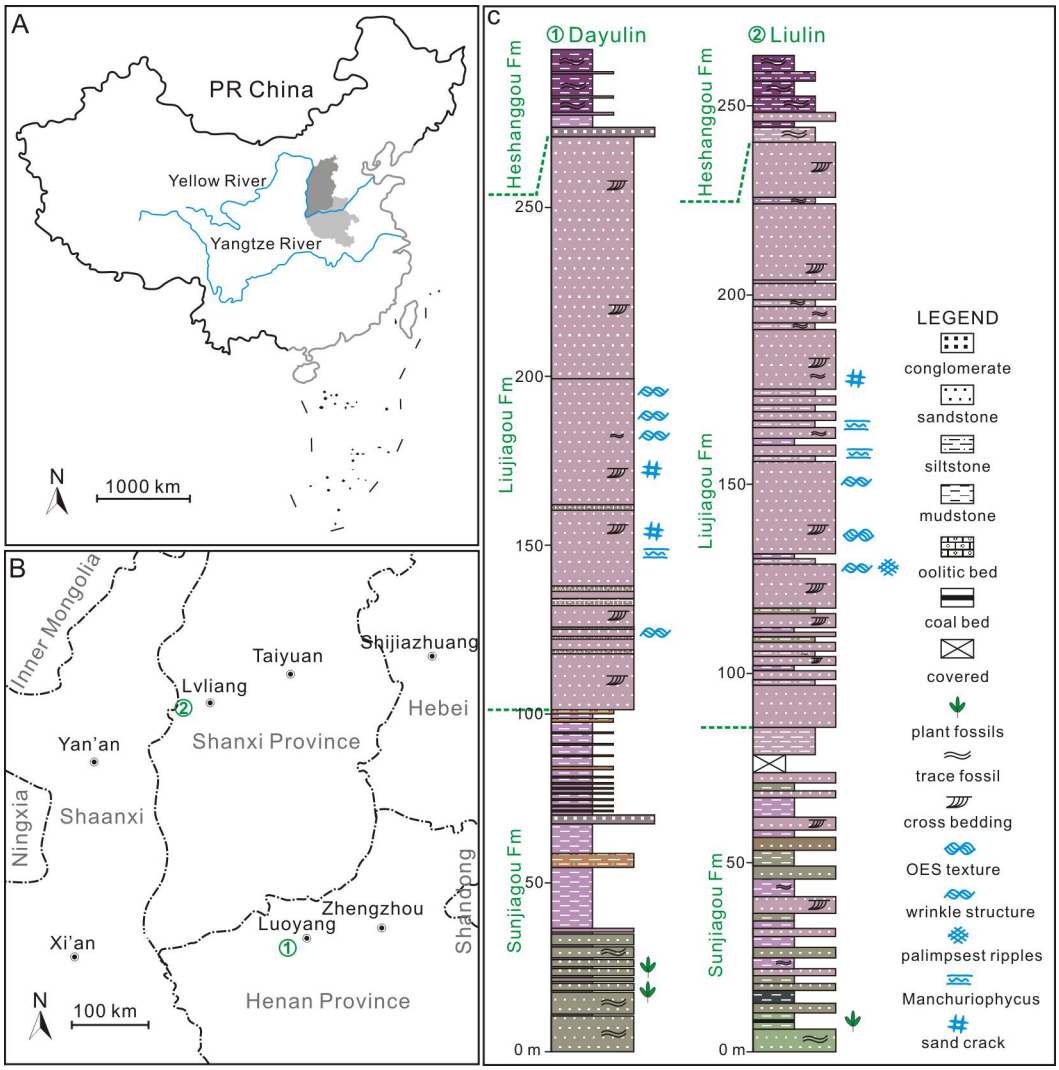
A
PR China
Yellow River
Yangtze River
N
1000 km
B
Inner Mongolia
Taiyuan
Shijiazhuang
Lvliang
Hebei
Yan'an
Shanxi Province
Ningxia
Shaanxi
Zhengzhou
Luoyang
Xi'an
Shandong
Henan Province
N
100 km
C
① Dayulin
② Liulin
Heshanggou Fm
Liujiagou Fm
Sunjiagou Fm
250
200
150
100
50
0 m
LEGEND
conglomerate
sandstone
siltstone
mudstone
oolitic bed
coal bed
covered
plant fossils
trace fossil
cross bedding
OES texture
wrinkle structure
palimpsest ripples
Manchuriophycus
sand crack

Fig. 1

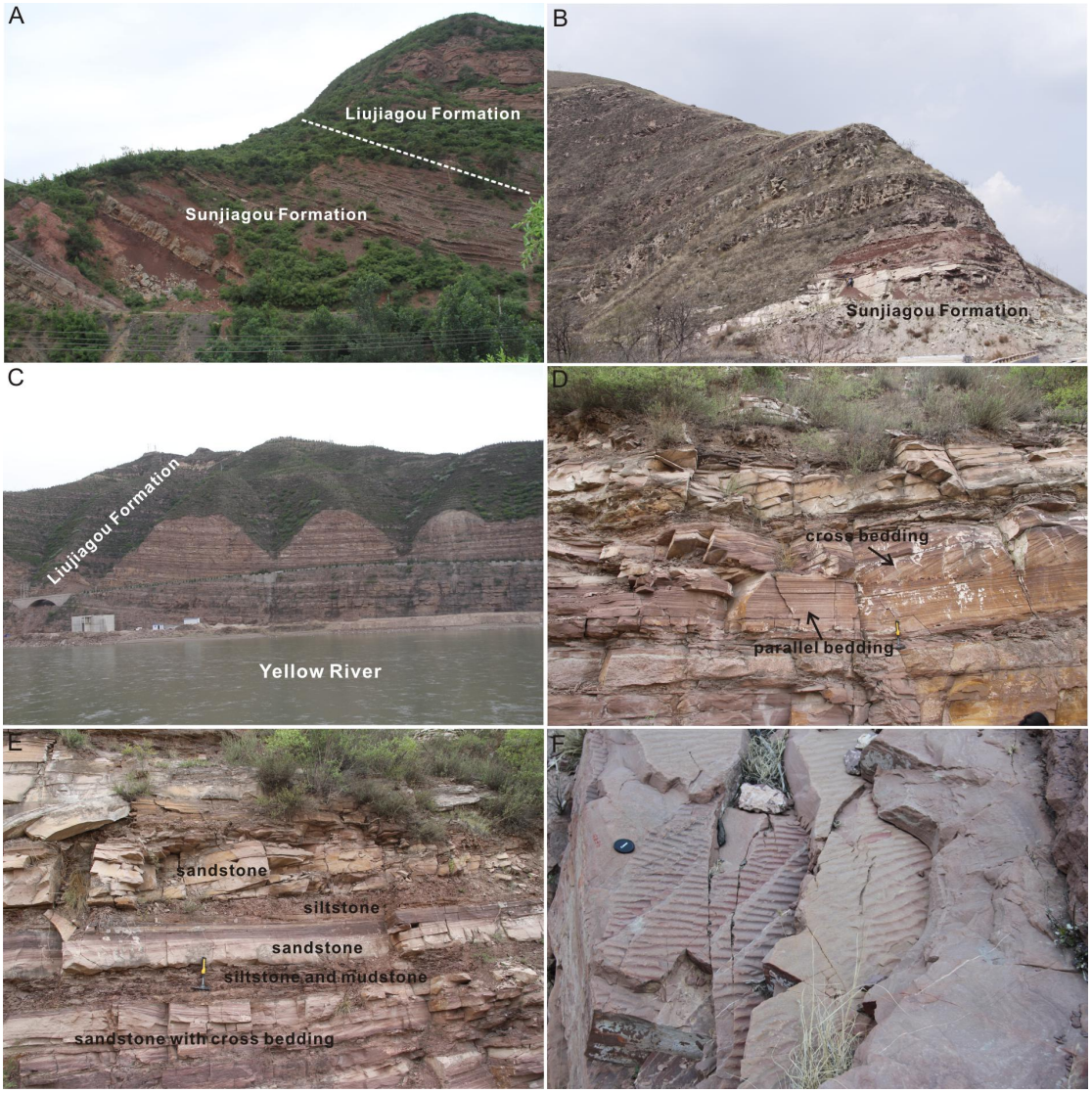
A
Liujiagou Formation
Sunjiagou Formation
B
Sunjiagou Formation
C
Liujiagou Formation
Yellow River
D
cross bedding
parallel bedding
E
sandstone
siltstone
sandstone
siltstone and mudstone
sandstone with cross bedding
F

Fig. 2

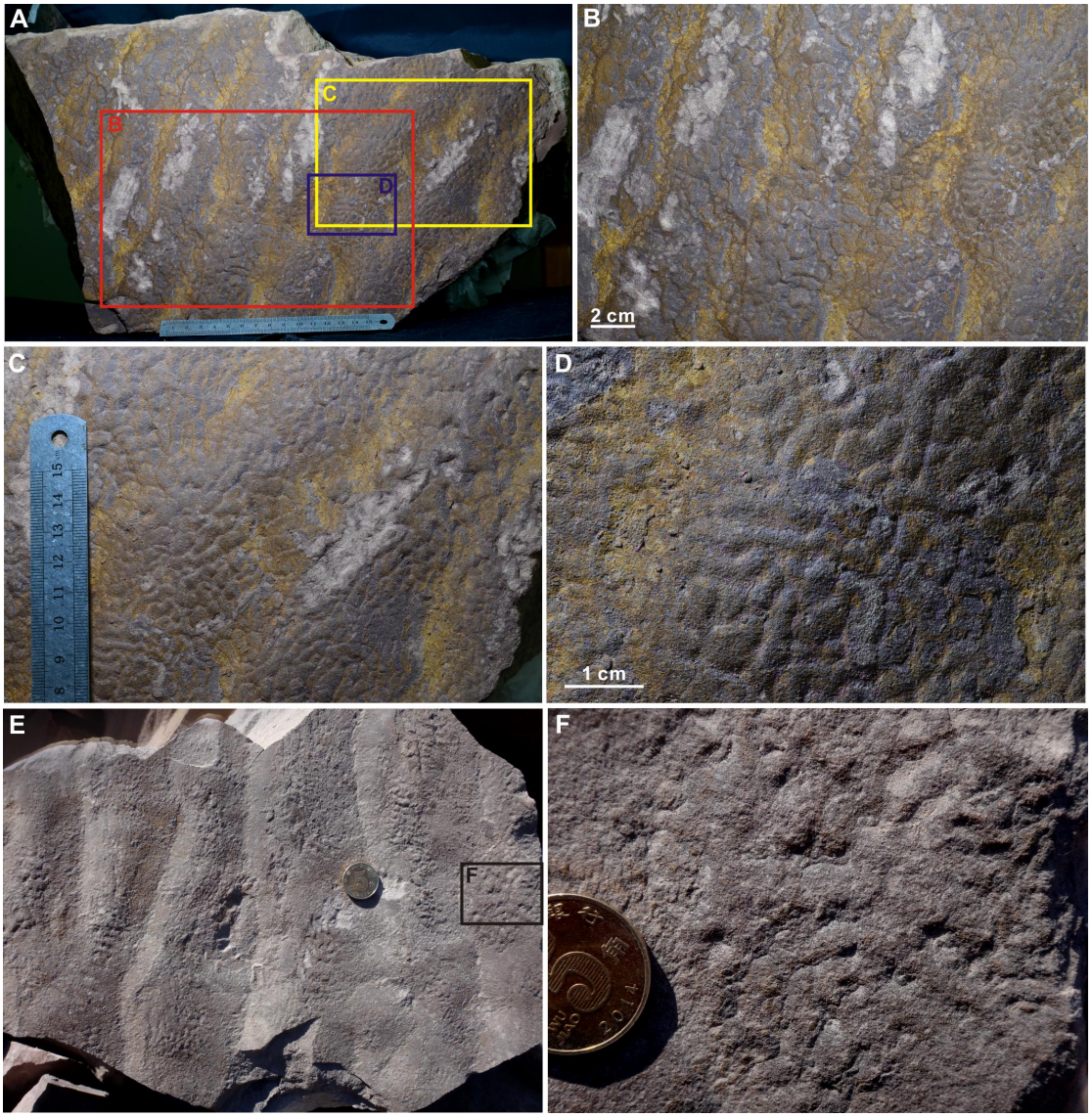

Fig. 3

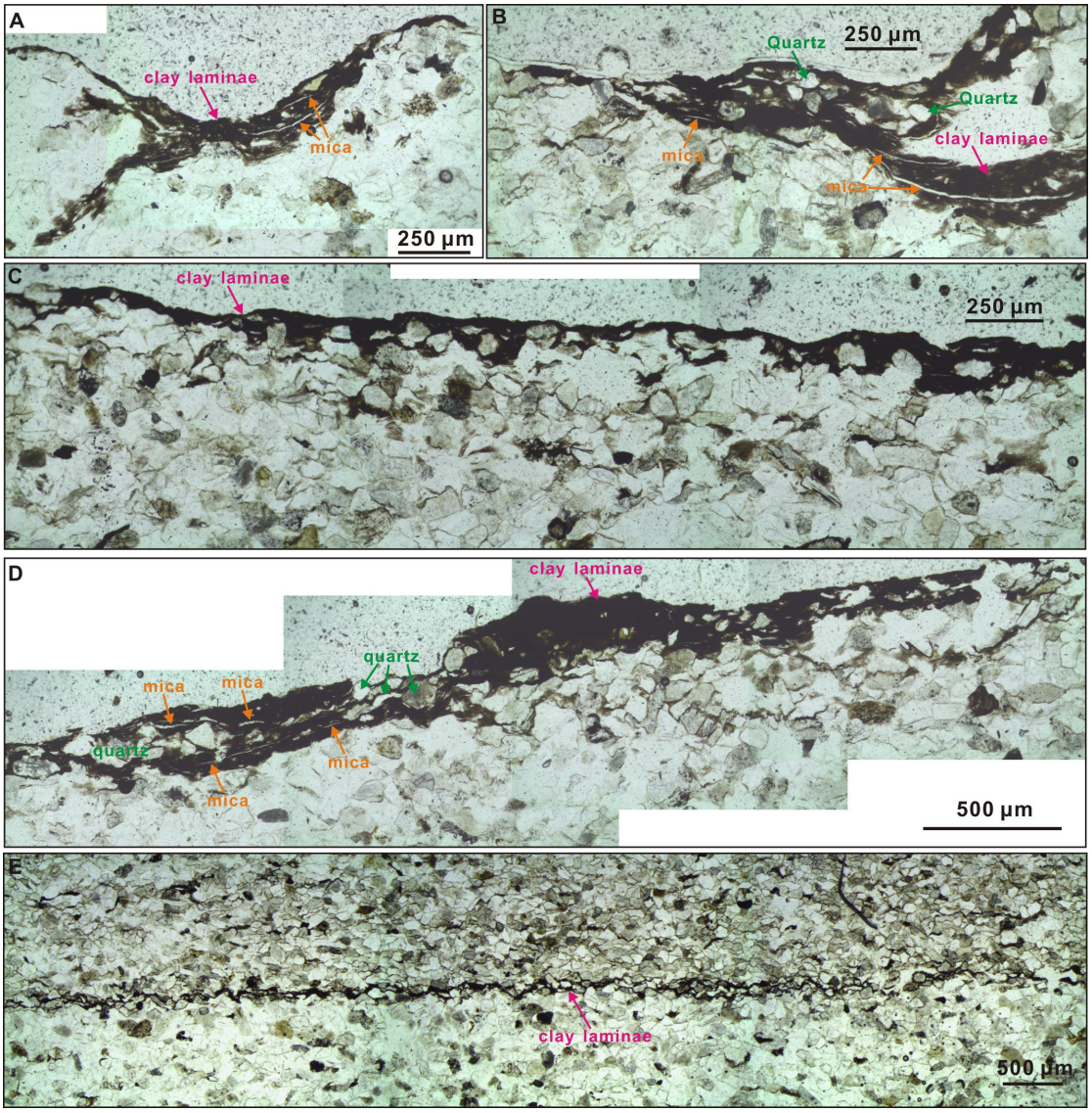
A
clay laminae
mica
250 µm
B
Quartz
250 µm
Quartz
clay laminae
mica
mica
C
clay laminae
250 µm
D
clay laminae
quartz
mica
mica
quartz
mica
mica
500 µm
E
clay laminae
500 µm

Fig. 4

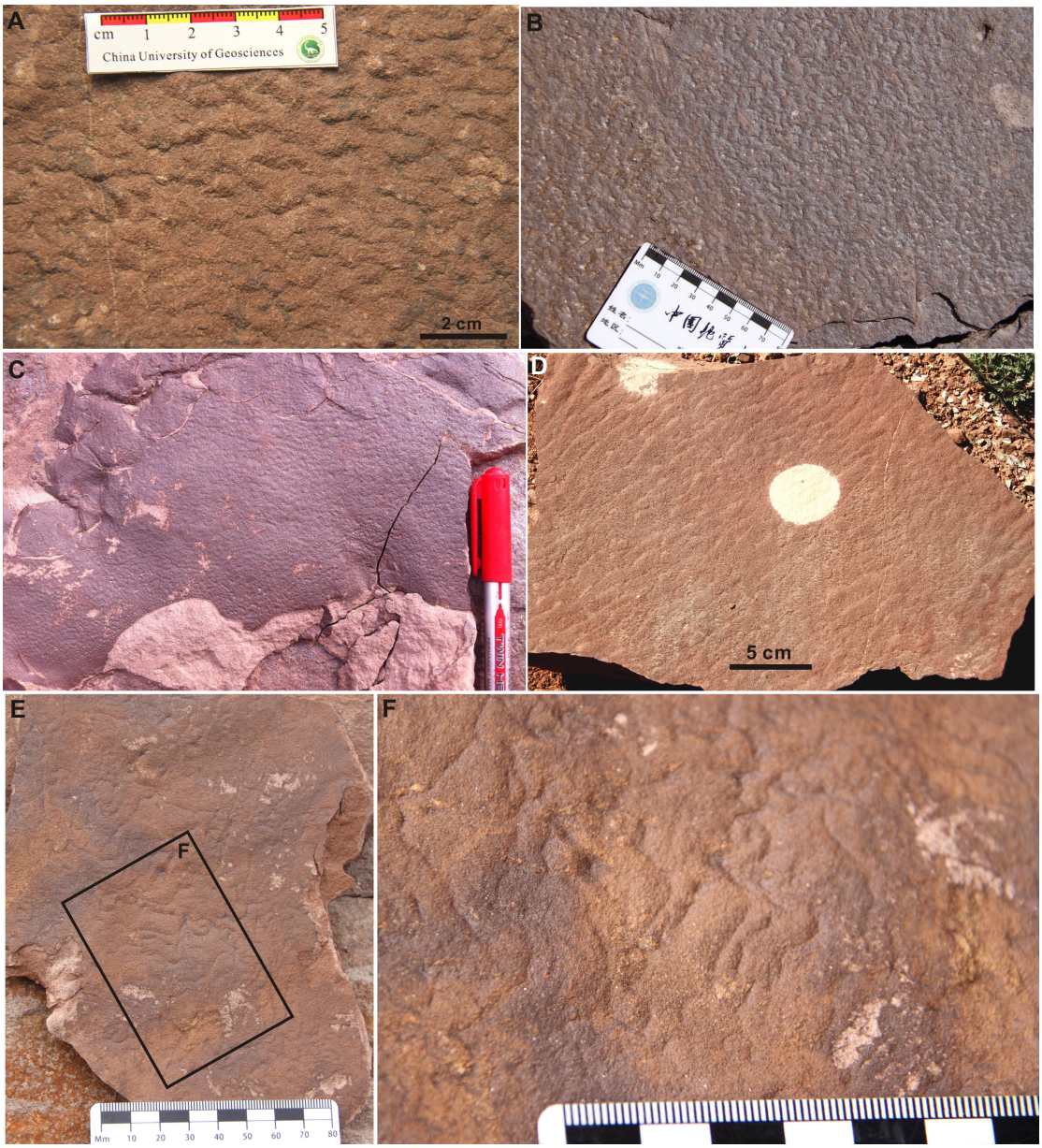

Fig. 5

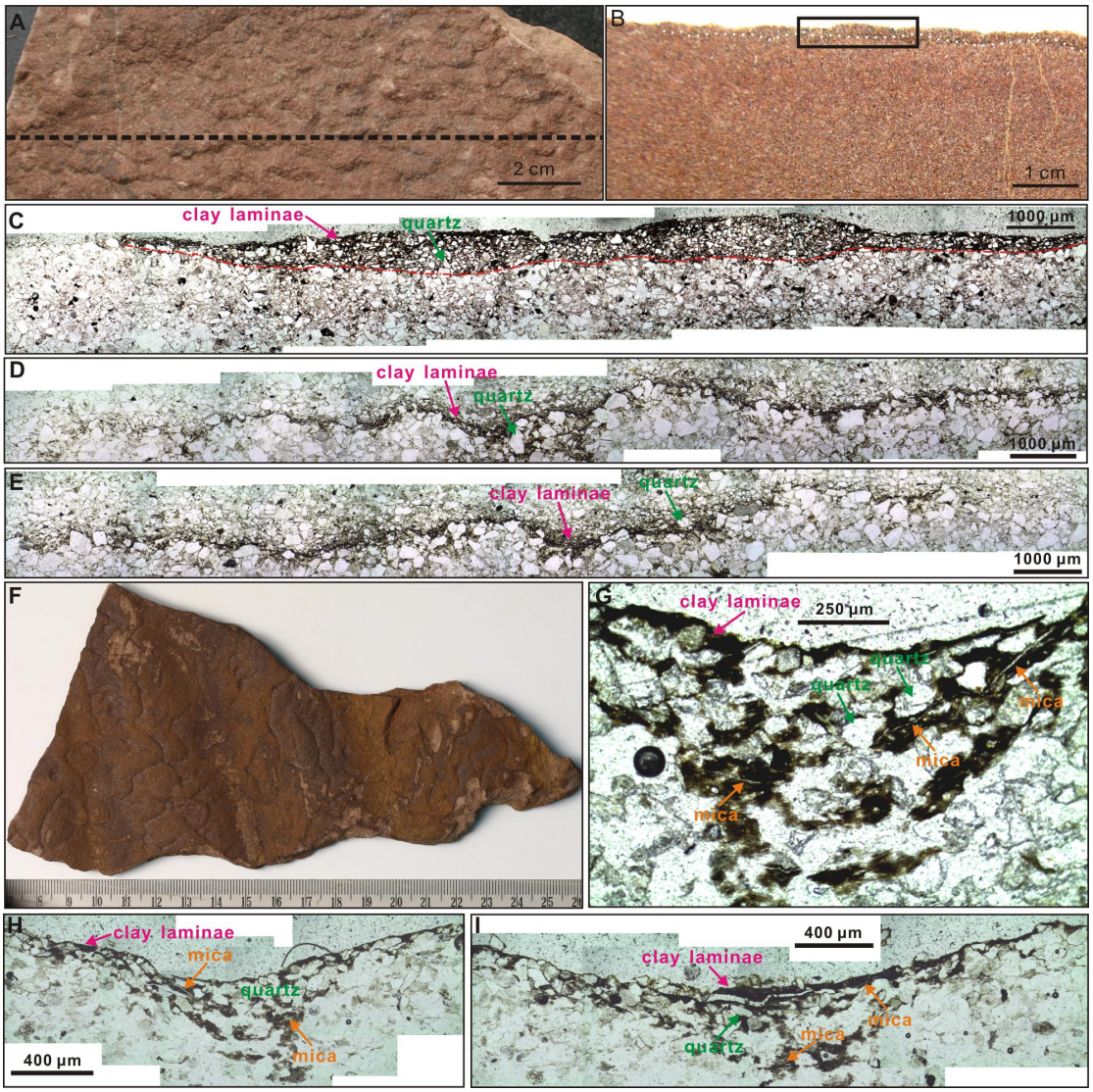
A
2 cm
B
1 cm
C
clay laminae
quartz
1000 µm
D
clay laminae
quartz
1000 µm
E
clay laminae
quartz
1000 µm
F
G
clay laminae
250 µm
quartz
quartz
mica
mica
mica
H
clay laminae
mica
quartz
mica
400 µm
I
400 µm
clay laminae
quartz
mica
mica

Fig. 6

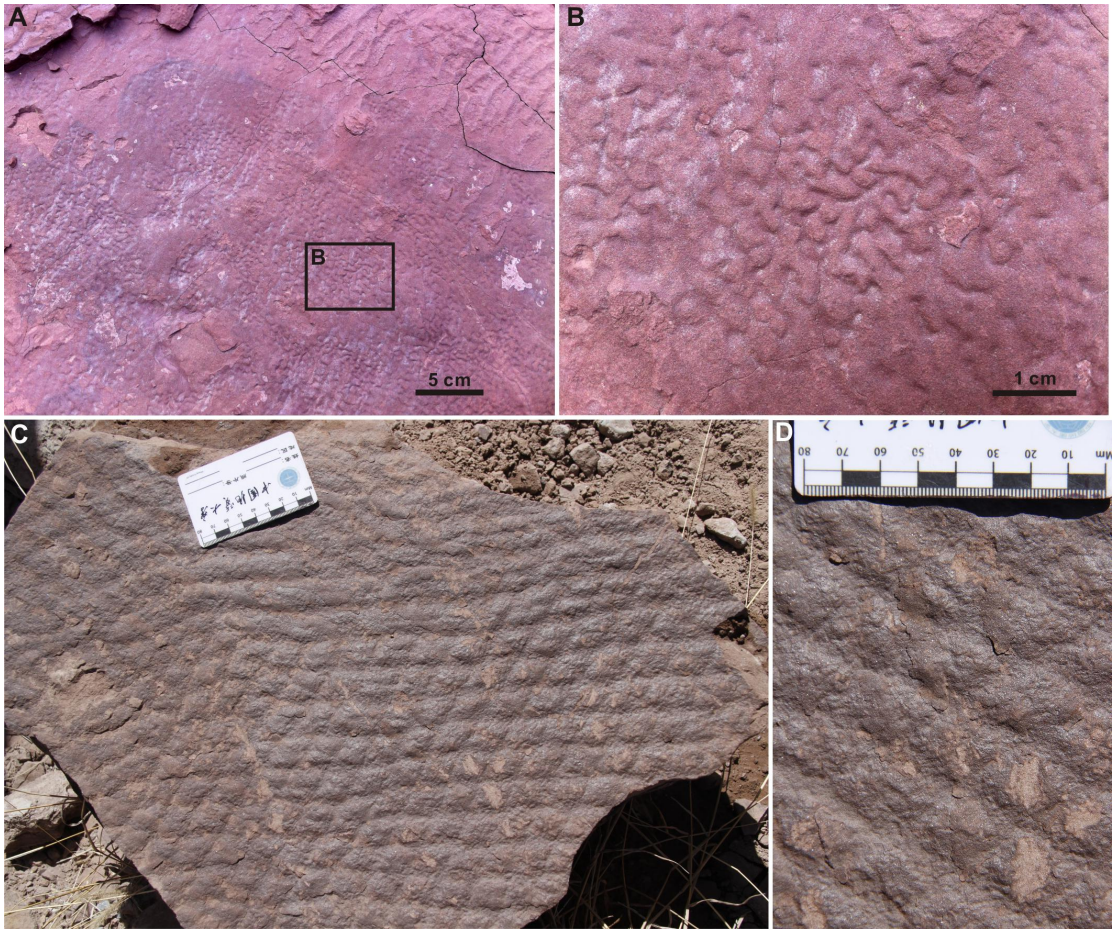

Fig. 7

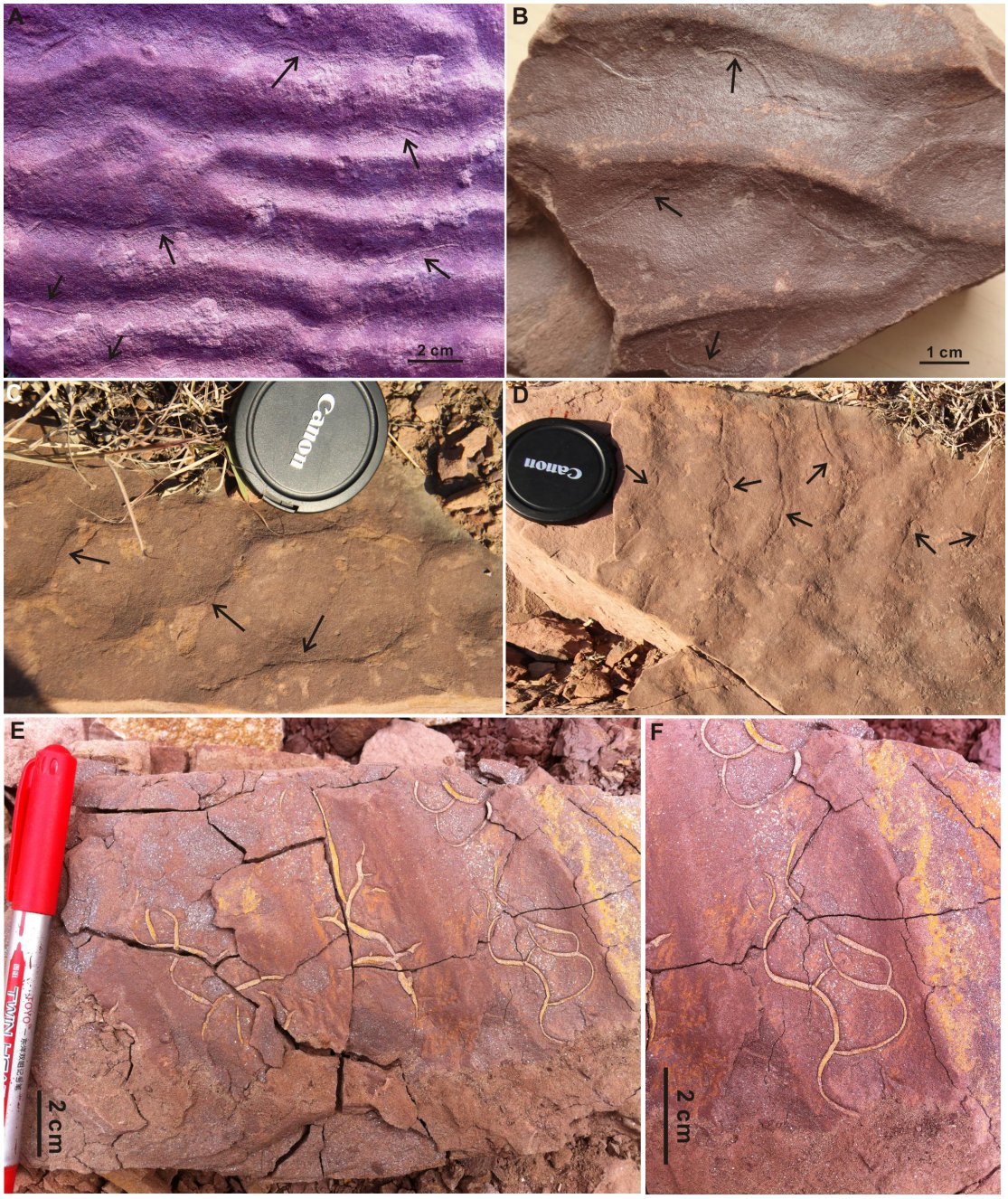

Fig. 8

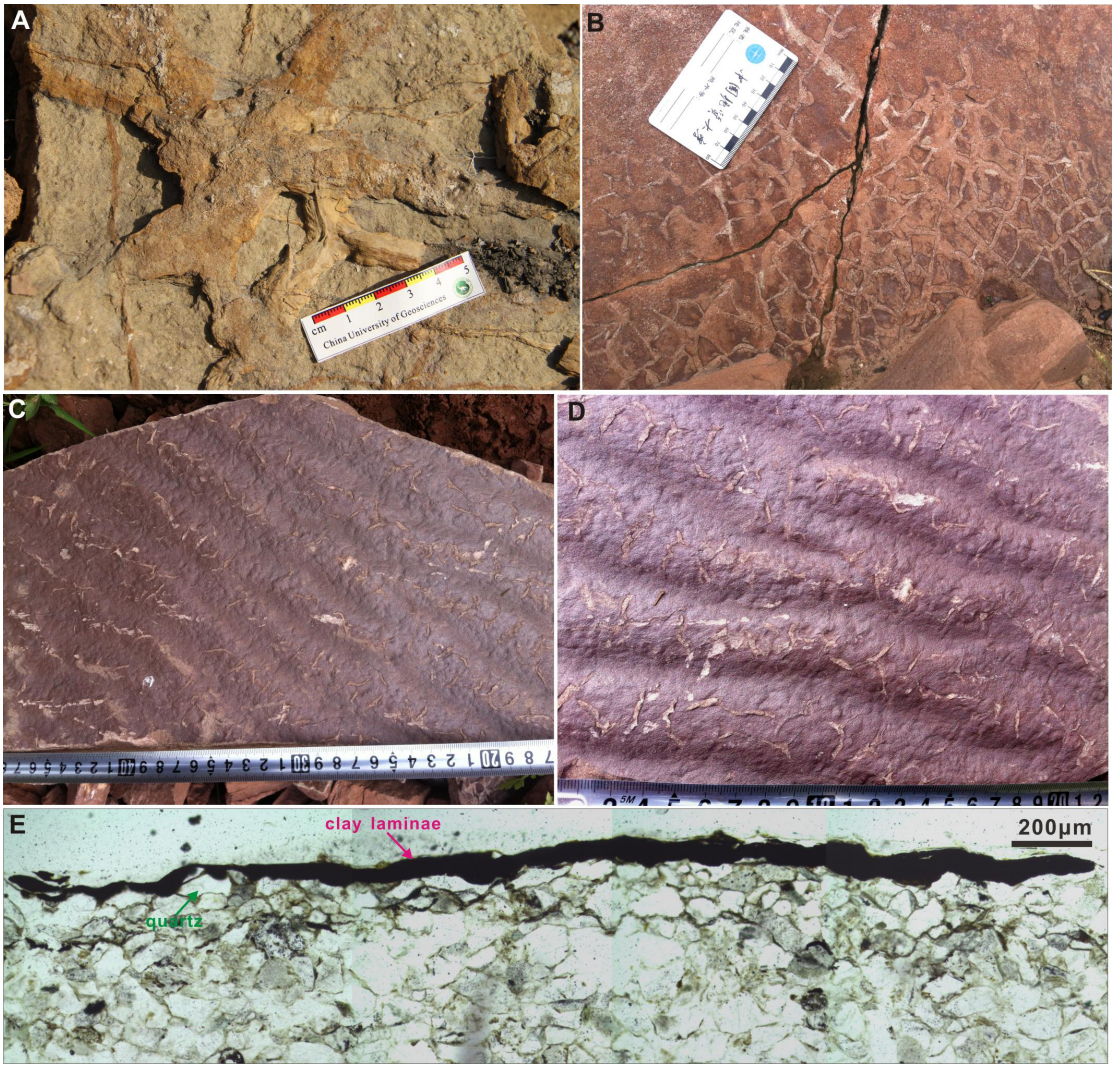

Fig. 9

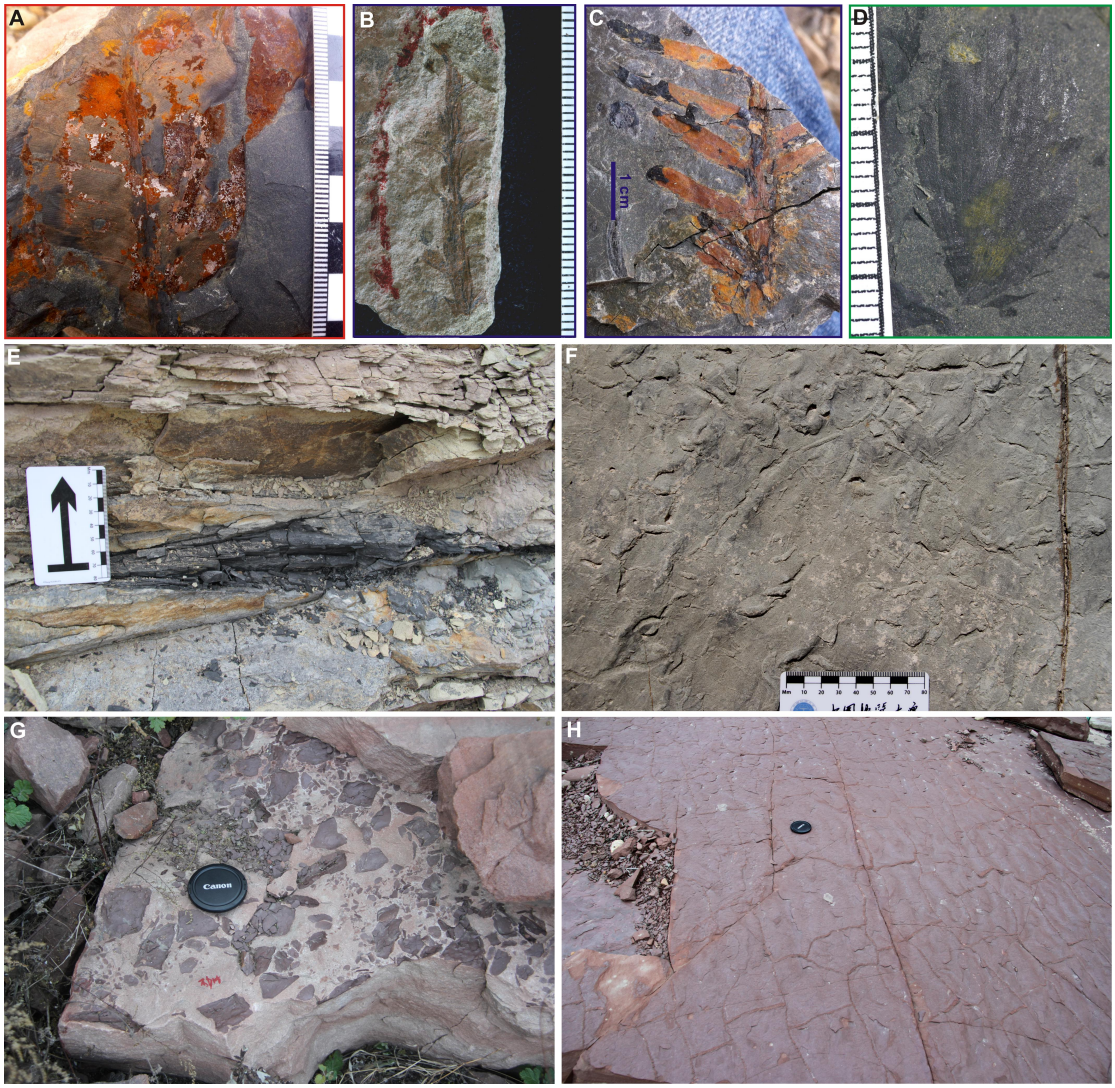

Fig. 10

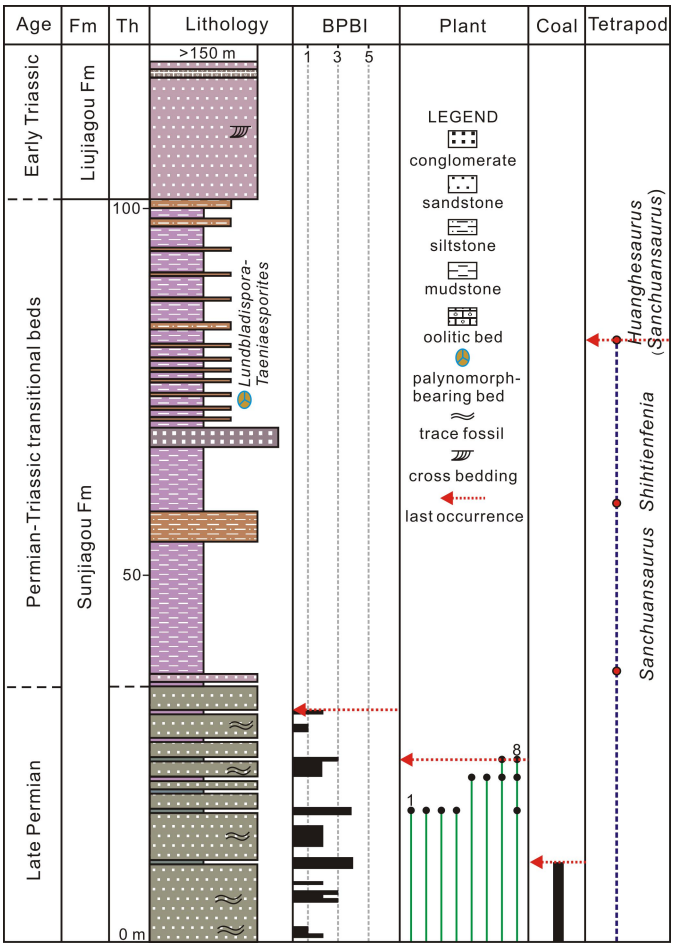
Age
Fm
Th
Lithology
BPBI
Plant
Coal
Tetrapod
Early Triassic
Liujiagou Fm
Permian-Triassic transitional beds
Sunjiagou Fm
Late Permian
>150 m
100
50
0 m
1
3
5
Lundbladispora-
Taeniaesporites
LEGEND
conglomerate
sandstone
siltstone
mudstone
oolitic bed
palynomorph-
bearing bed
trace fossil
cross bedding
last occurrence
8
1
Huanghesaurus
(Sanchuansaurus)
Shihtienfenia
Sanchuansaurus

Fig. 11

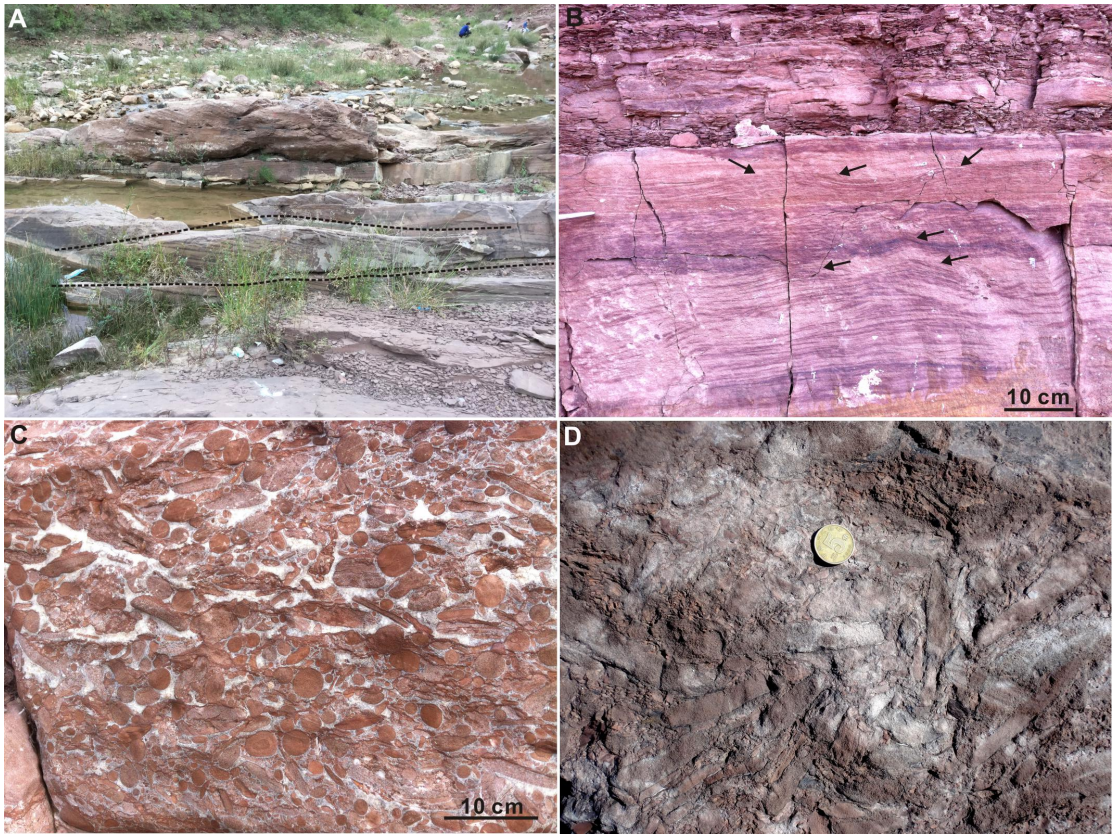

Fig. 12

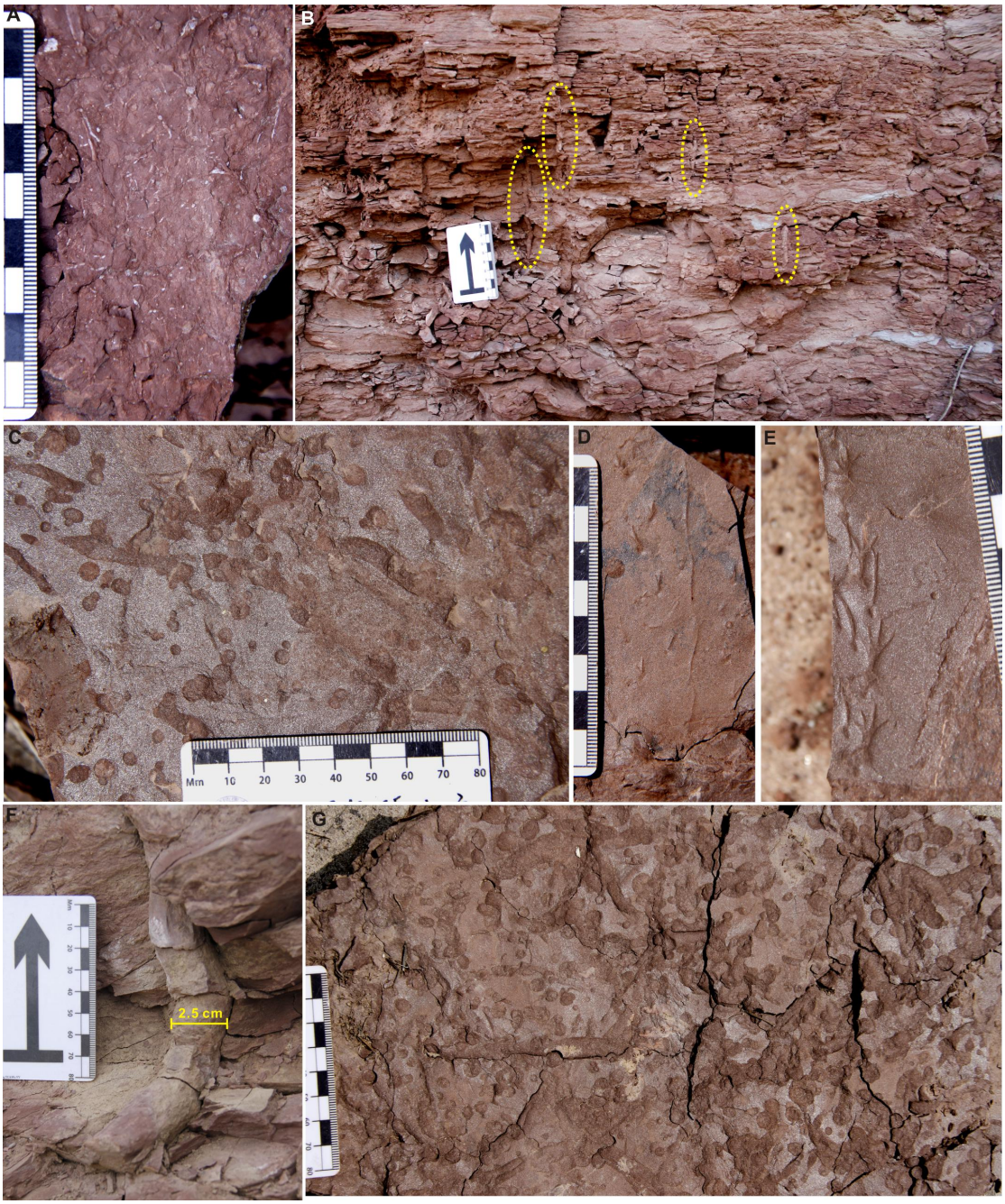

Fig. 13